Recent advances in aptamer applications for analytical biochemistry

Gerald Zon

TriLink BioTechnologies, 10770 Wateridge Circle, Suite 200, San Diego, CA, 92121, USA

ARTICLE INFO

ABSTRACT

Aptamers are typically defined as relatively short (20–60 nucleotides) single-stranded DNA or RNA molecules that bind with high affinity and specificity to various types of targets. Aptamers are frequently referred to as "synthetic antibodies" but are easier to obtain, less expensive to produce, and in several ways more versatile than antibodies. The beginnings of aptamers date back to 1990, and since then there has been a continual increase in aptamer publications. The intent of the present account was to focus on recent original research publications, i.e., those appearing in 2019 through April 2020, when this account was written. A Google Scholar search of this recent literature was performed for relevance-ranking of articles. New methods for selection of aptamers were not included. Nine categories of applications were organized and representative examples of each are given. Finally, an outlook is offered focusing on "faster, better, cheaper" application performance factors as key drivers for future innovations in aptamer applications.

1. Introduction

Aptamers are typically defined [1] as relatively short (20–60 nucleotides) single-stranded DNA or RNA molecules that bind with high affinity and specificity to various types of targets, such as small molecules, peptides, proteins, cells, and tissues. Aptamers are frequently referred to as "synthetic antibodies" [2] but are easier to obtain, less expensive to produce, and in several ways more versatile than antibodies, which are attributes that have led to the view [3] of aptamers as replacing antibodies in many applications.

The beginnings of aptamers date back to 1990 when, by remarkable coincidence, two labs—Tuerk and Gold [4] and Ellington and Szostak [5]—independently published the conceptually similar achievement of selecting RNA sequences that bind to specific target molecules, i.e. aptamers—a term coined two years later [6]. Although somewhat different technical approaches were used, both started with highly complex mixtures of synthetic RNA having "random sequence" (A/G/C/U) regions. The procedure described by Tuerk and Gold [4], which was referred to as "systematic evolution of ligands by exponential enrichment" (SELEX), has ~9100 citations in Google Scholar [7] as of April 2020. The alternative selection strategy reported by Ellington and Szostak [5] has likewise had a major impact, as reflected in ~8400 citations in Google Scholar during this same time.

A better measure of the impact of aptamers following these two seminal publications can be obtained from major databases of scientific publications such as PubMed [8], which comprises over 30 million citations for the fields of biomedicine, health, and portions of chemical sciences and bioengineering, but not patents. Information on patents and additional chemistry sources are contained in SciFinder [9], which currently contains over 47 million records that are maintained by Chemical Abstracts Service. Both of these databases, which have some overlap, are freely available and easy to search in various ways. For example, Fig. 1 is a chart of annual publications in PubMed that are indexed to the term aptamer during 1992–2019, with aptamer appearing in any field, e.g. title, abstract, text, etc. These results clearly show a continual increase, on average, and represent a total of ~10,500 publications, with ~1400 in 2019 alone—nearly 4 per day.

The ACS SciFinder database has ~29,000 references indexed to aptamers for this same period, 1992–2019, wherein there are ~4800 patents, ~1000 conference proceedings, and ~250 dissertations. Google Scholar gave ~88,000 results—including patents and citations—for this period, with aptamer anywhere in the article, and ~8500 with aptamer in the title. Collectively, all of these impressively large numbers related to aptamers underscore the magnitude of the impact that aptamers have had, and will continue to have in the future, based on the historical trend evident in Fig. 1. As a final note on resources, recently launched *Aptamers*—the official open-access journal of the International Society on Aptamers—will consider and publish peer-reviewed studies on all aspects of aptamer research.

Mindful of this vast amount of published literature related to aptamers, and the ability to filter the content of the PubMed database, the intent of the present review was to focus on recent publications, i.e.,
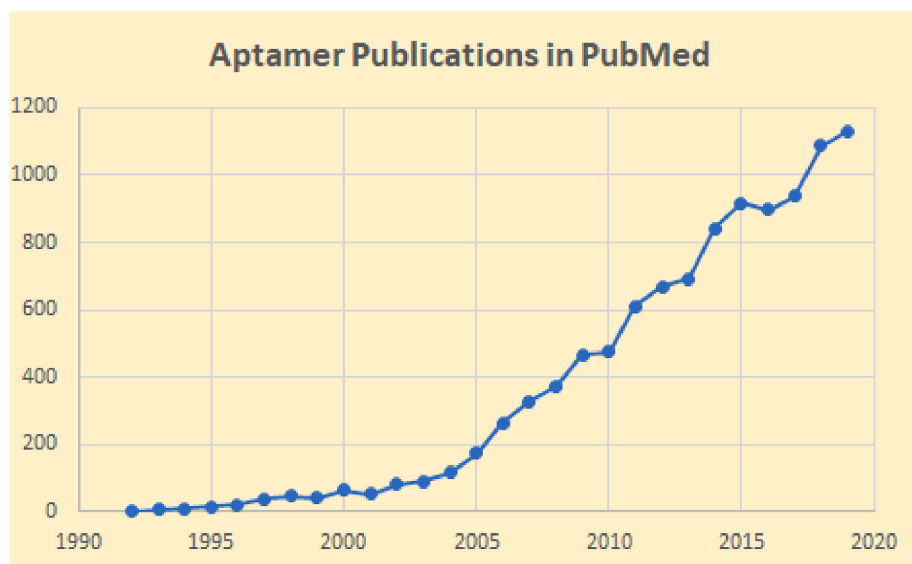
Fig. 1. Chart of annual publications in PubMed that are indexed to the term aptamer during 1992–2019, with aptamer appearing in any field.

those appearing in 2019 through April 2020, when this account written. Patent literature, although very important for commercialization, was intentionally omitted. A Google Scholar search was also performed to find items that contained the term aptamer with application-related words, such as sensors, electrochemical, fluorescent, targeting, delivery, diagnostics, proteins, food safety, etc. in a Boolean "OR" manner.

Methods for selection of aptamers and methods for attachment of aptamers to gold surfaces were not directly searched, as recent reviews for each topic are available (e.g. [10,11]). The resultant ˜500 items, derived and rank-order listed by Google Scholar according to its algorithms, were then perused for selection, sorting, and organization (Fig. 2). Also, and with apologies to the many aptamer researchers not

Fig. 2. Graphical outline of clockwise content headings for sections 2.-10.

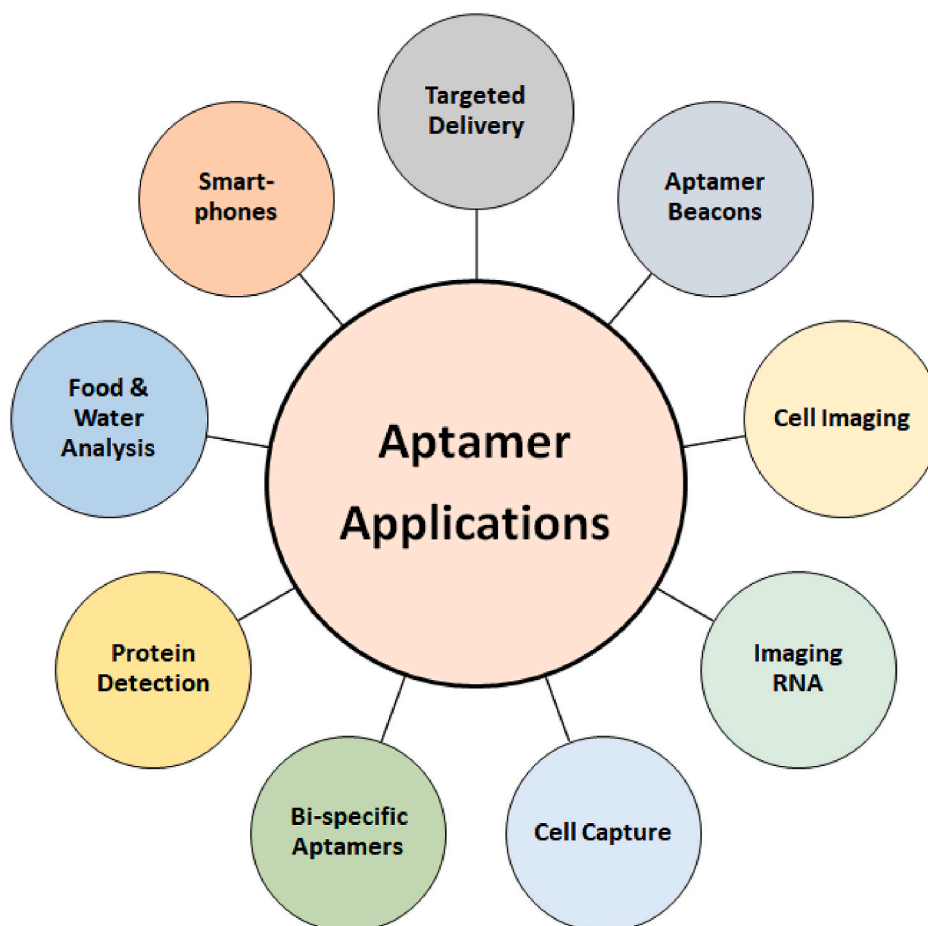cited herein, the following account is by no means intended to be comprehensive, and its contents unavoidably reflect subjective biases of this author.

2. Targeted delivery

The vast majority of publications on targeted delivery involve various aspects of therapeutics, primarily cancer. Several reviews are available, e.g. those by Shigdar [12], Zununi Vahed et al. [13], and Moosavian et al. [14], the latter of which covers aptamer-functionalized liposome platforms. Also, there is a book chapter by Eilers et al. [15] titled *Aptamer-Modified Nanoparticles in Medical Applications*. Selected original research publications include the following. The following six examples were selected to illustrate the wide diversity of recent approaches for targeted delivery enabled by aptamers. These include lipid or polysaccharide nanocarriers loaded with either nucleic acid therapeutics or conventional drugs or both, and carrying moieties for detection, i.e. theranostics.

Kim et al. [16] reported that hydrophobic quantum dots (QDs) [17] were effectively incorporated into lipid bilayers, and then therapeutic short-interfering RNAs (siRNAs) [18] were complexed with QD-lipid nanocarriers (QLs). Anti-epidermal growth factor receptor [19] (EGFR) aptamer-lipid conjugates were inserted into the QLs for triple-negative breast cancer (TNBC) targeting. These TNBC-targeted constructs, aptamo-QLs, were directly compared to anti-EGFR antibody-coupled immuno-QLs. The in vitro delivery of therapeutic siRNAs and QDs to target cells was assessed by flow cytometry and confocal microscopy. The in vivo targeting of siRNAs to tumors and therapeutic efficacy were evaluated in mice carrying tumors derived from a human breast adenocarcinoma cell line. Both types of EGFR-targeting QLs showed enhanced delivery to target cancer cells, resulting in more effective gene silencing and enhanced tumor imaging compared to non-targeting control QLs. Moreover, combinatorial therapy with Bcl-2 and PKC-iota siRNAs loaded into the anti-EGFR QLs was said to be remarkably effective in inhibiting tumor growth and metastasis, leading to the conclusion that these anti-EGFR aptamer-guided lipid carriers may be a potential theranostic delivery vehicle for RNA interference and fluorescence imaging of TNBCs. For a 2020 review of recent advances in theranostic polymeric nanoparticles for cancer treatment, see Indoria et al. [20].

Zou et al. [21] described targeting of exosomes (Exos), which are nanoscale natural vehicles for transporting biomolecules to facilitate cell-to-cell communication [22]. To improve the delivery efficiency of Exos, these researchers used diacyllipid-polyethyleneglycol (PEG)-aptamer conjugates as the targeting ligand to develop an aptamer-functionalized Exos (Apt-Exos) platform for cell type-specific delivery of molecular therapeutics (Fig. 3). The 48-mer DNA aptamer can specifically recognize membrane-expressed protein tyrosine kinase 7, as previously reported [23]. The cellular uptake mechanism of Apt-Exos was investigated in detail using endocytosis modulators, dyes for microscopic visualization, and flow cytometry, compared to free Exos. To engineer the Apt-Exos as a drug delivery system, doxorubicin (Dox), a commonly used anticancer drug, was used as the drug model and loaded into Exos through electroporation. The cell-type-specific accumulation and cytotoxicity of Dox via the Apt-Exos construct (APT-Exos-D) were demonstrated by standard techniques. The authors concluded that Apt-Exos can efficiently deliver molecular drugs/fluorophores to target cancer cells, providing a promising delivery platform for cancer theranostics.

Zhong et al. [24] investigated aptamer-based targeting of papillary thyroid carcinoma (PTC), which is of high incidence worldwide, and the prognosis for patients with advanced PTC is poor. Prior to this investigation, there was no specific biomarker that can identify PTC, and there were deficiencies in existing diagnostic methods. An 80-mer DNA aptamer, termed TC-6, was generated from tissue-SELEX [25] using sections of PTC and a normal thyroid gland. TC-6 could specifically
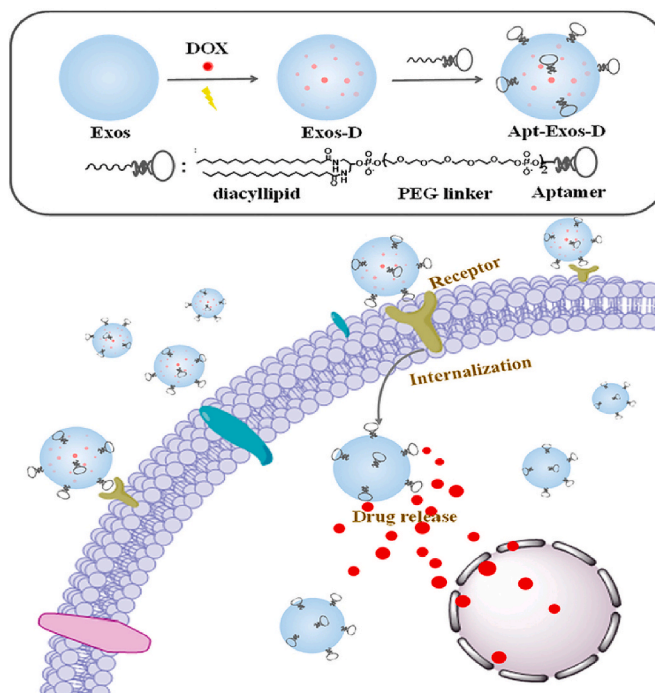

Fig. 3. Illustration of construction and targeted delivery of aptamer-functionalized drug-loaded Exos (Apt-Exos-D). Exos were loaded with the chemotherapeutic drug doxorubicin (Dox) via electroporation. The drug-loaded Exos (Exos-D), which were functionalized with an aptamer (Apt-Exos-D), can efficiently deliver Dox to target cancer cells for enhanced cancer chemotherapy. Taken from Zou et al. Anal. Chem. 2019, 91, 3, 2425–2430 [21] with permission. Copyright © 2019 American Chemical Society.

target intracellular components of PTC cells with $K_d = 58$ nM, and exhibited good biostability both in vitro and in vivo. Moreover, fluorescence imaging of PTC tumor-bearing mice revealed that TC-6 was able to accumulate in tumor sites and could distinguish thyroid carcinoma from other benign thyroid tissue. In addition, TC-6d, a 60-mer truncated aptamer of TC-6, maintained its affinity toward PTC with a $K_d = 39$ nM. It was concluded that, overall, these results indicate that TC-6 is a potential candidate for developing novel tools for diagnosis and targeted therapy of PTC.

According to a recent review [26], nucleolin is one of the most abundant non-ribosomal phosphoproteins of nucleoli. However, in several cancers, nucleolin is highly expressed both intracellularly and on the cell surface, which led to the development of the aptamer AS1411, a 26-base guanine (G)-rich quadruplex oligodeoxynucleotide [27] (Fig. 4) that has been PEGylated for clinical studies [28]. Through binding to cell surface nucleolin, AS1411 is internalized and may prevent nucleolin from binding to and stabilizing mRNA of anti-apoptotic BCL2 [29] protein, thereby destabilizing BCL2 mRNA, leading to a reduction in BCL2 protein synthesis. This can then lead to the induction of apoptosis. As might be expected, there have been a number of investigations of AS1411-based targeting, with at least 13 such publications during 2019–April 2020 found in PubMed by searching "AS1411".

For example, Yu et al. [30] reported that an AS1411-functionalized liposome can simultaneously deliver paclitaxel (PTX), a drug used to treat breast and other of types of cancer, and Polo-like kinase-1 [31] (PLK-1)-targeted siRNA into MCF-7 breast cancer cells in vitro and in vivo. The simultaneous delivery of PTX and the anti-PLK-1 siRNA synergistically increased the number of apoptotic cells and reduced angiogenesis, relative to liposomal delivery of PTX and the anti-PLK-1 siRNA separately. It was concluded that simultaneous delivery of PTX and PLK1-targeted siRNA using AS1411 aptamer-functionalized liposomes has potential clinical value for therapy of breast cancer.
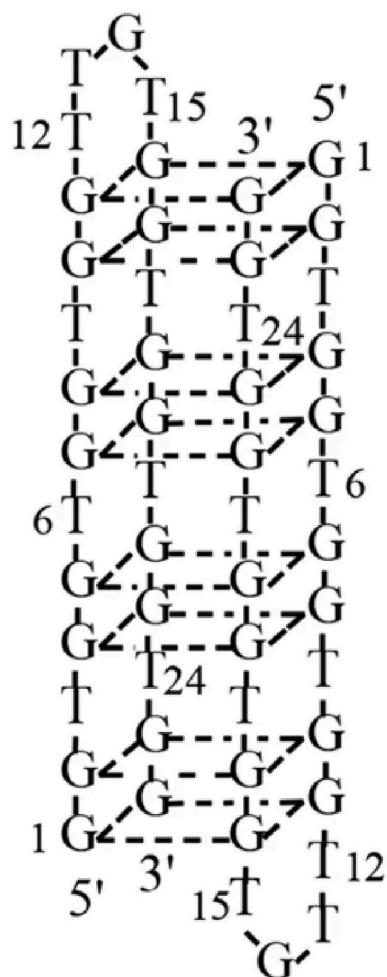
Fig. 4. Secondary structure of AS1411. Taken from Fan et al. [27] Sci. Rep. 2016, 6, 25,799 with permission. Copyright © 2016 Springer Nature.

Another noteworthy example involves theranostics using carbon dots (CDs) [17], which are a relatively new class of fluorescent carbon nanomaterials that have proven to be powerful tools in the field of bioimaging and biosensing due to their small size, photostability and favorable biocompatibility. Kong et al. [32] assembled CDs coated with positively-charged polyethyleneimine (PEI), followed by conjugation with AS1411 through electrostatic interactions to form CDs-PEI-AS1411 nanocomplexes. The cytotoxicity of the CDs-PEI-AS1411 and CDs-PEI constructs was assayed in two cancer cell lines, breast MCF-7 (high nucleolin level) and fibroblast L929 (low nucleolin level), and the cellular uptake of CDs-PEI-AS1411 was studied with confocal microscopy and flow cytometry. The constructs showed good photostability and no obvious cytotoxicity. The cellular uptake of the CDs-PEI-AS1411 nanocomplex in MCF-7 cells was significantly higher than that of L929 cells, consistent with nucleolin-mediated uptake. It was concluded that the CDs-PEI-AS1411 construct has potential utility in nucleolin-related cancer cell targeted imaging.

Finally, Alizadeh et al. [33] coated chitosan (CS), a drug-carrier crustacean-derived polysaccharide [34], on silica (SiO2@CS) nanoparticles (NPs) and attached them to epigallocatechin gallate (EGCG), which a natural product from green tea that is reported [35] to modulate cancer immunity. The amine groups of chitosan in SiO2@CS-EGCG NPs (~100 nm) were used to attach the AS1411 aptamer electrostatically. The internalization efficiency of SiO2@CS-EGCG-aptamer NPs (51%) was higher than SiO2@CS-EGCG NPs (29%) in the ovarian cancer SKOV-3 cell line, consistent with recognition of nucleolin by the attached AS1411 aptamer. In addition, DAPI staining and Annexin V

analyses showed that SiO2@CS-EGCG-aptamer NPs improved the cytotoxic effect of the EGCG, with ~93% of cells showing late apoptosis. These results suggested the potential utility of this novel type of silica-based construction for other aptamer-targeted applications.

3. Aptamer beacons

Nearly two decades ago, Hamaguchi et al. [36] described a new class of molecules, dubbed "aptamer beacons", for detecting a wide range of ligands. In their design strategy (Fig. 5), similar to molecular beacons [37], aptamer beacons can adopt two or more conformations, one of which allows ligand binding. A fluorescence-quenching pair is used to report changes in conformation induced by ligand binding. As an example of an aptamer beacon, an anti-thrombin aptamer was engineered into an aptamer beacon by adding nucleotides to the 5′-end which are complementary to nucleotides at the 3′-end of the aptamer. In the absence of thrombin, the added 5′-end nucleotides will form a duplex with the 3′-end, forcing the aptamer beacon into a stem-loop structure. In the presence of thrombin, the aptamer beacon forms the ligand-binding structure. This conformational change causes a change in the distance between a fluorophore attached to the 5′-end and a quencher attached to the 3′-end, thus leading to unquenching and "light-up" detection.

There are now more than 30 reports in PubMed indexed to aptamer beacons in the title and/or abstract, seven of which have been published in the past five years and include a review in 2019 by Moutsiopoulou et al. [38]. Of these recent examples, the three given in the next paragraphs were selected because they involve detection of adenosine triphosphate (ATP), which—as an analyte—has been the subject of at least 11 reports during 2019–April 2020 in PubMed having ATP and aptamer in the title. This notable amount of attention to ATP derives from the fact that ATP concentrations can be associated with various cellular conditions or "states".

According to Peng et al. [39], abnormal concentrations of ATP are associated with many diseases and cancers, and quantitative detection of
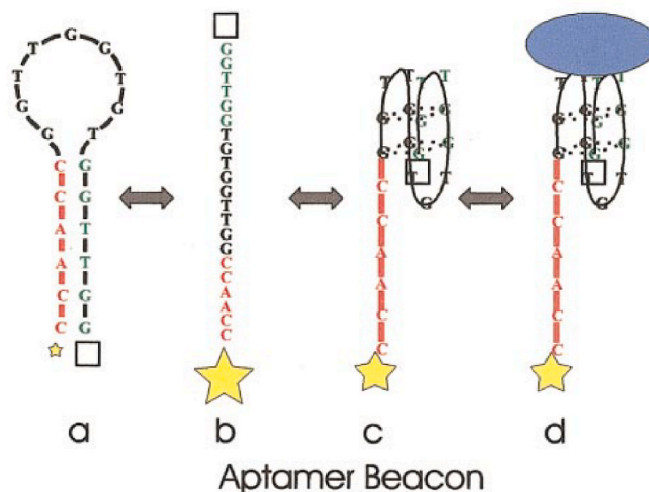
Fig. 5. Aptamer beacon—schematic drawing of the mechanism of signaling by a thrombin aptamer beacon. (a) Aptamer beacon in quenched stem-loop conformation. Yellow stars represent the fluorophore, and the white square represents the quencher. The emission intensity of the fluorophore is represented by the size of the star, and increases with the distance between the fluorophore and the quencher. (b) Unfolded conformation. (c) Aptamer in G-quadruplex conformation that allows thrombin binding. (d) Thrombin bound to aptamer beacon. Taken from Hamaguchi et al. [36] Anal. Biochem. 2001, 294, 126–131 with permission. Copyright © 2001 Academic Press. Note: In the original publication [36], the caption text for (a)–(d) was accidently reversed from the correct order given here. (For interpretation of the references to color in this figure legend, the reader is referred to the Web version of this article.)

ATP is thus of great importance for disease diagnosis and prognosis. These researchers developed a new dual recycling amplification sensor integrated with catalytic hairpin assembly (CHA) [40] to achieve high sensitivity for fluorescent detection of ATP. The association of the target ATP with the aptamer beacons causes the allosteric structure switching of the aptamer beacons to expose the "toehold" regions, which hybridize with and unfold the fluorescently quenched hairpin signal probes (HP1) to recycle the target ATP and to trigger CHA between HP1 and the secondary hairpin probes (HP2) to form HP1/HP2 duplexes. Due to the recycling amplification, the presence of ATP leads to the formation of many HP1/HP2 duplexes, generating dramatically amplified fluorescent signals for sensitive detection of ATP. This sensor linearly responds to ATP in the range from 25 to 600 nM with a calculated limit of detection (LOD) of 8.2 nM. Furthermore, the sensor shows high selectivity and can also be used to detect ATP in human serum.

More recently, Xu et al. [41] achieved ~4-fold lower LOD in the following manner by coupling extension/excision amplification with target recycling. The ATP target molecules associate with aptamer-containing double-hairpin probes and cause conformational changes of the probes to initiate the cyclic strand extension/excision processes in the presence of polymerase, endonuclease and assistance sequences for the recycling of ATP and the production of a large number of G-quadruplex sequences. The organic dye thioflavin T subsequently binds these G-quadruplex sequences to yield substantially enhanced fluorescence emission for achieving highly sensitive detection of ATP down to 2.2 nM.

Subsequently, Feng et al. [42] detected ATP by use of adsorption of a 5′-fluorescein-labeled aptamer specific for ATP to graphene oxide, which causes fluorescence quenching that is unquenched in the presence of increasing concentrations of ATP. For this system, the ATP-specific aptamer was synthesized in either the natural nuclease-sensitive D-DNA form or the unnatural nuclease-resistant mirror image L-DNA form (section 5.2). Both forms were found to have the same unquenching activities, and the L-DNA form is therefore more advantageous for ATP detection in the presence of nucleases.

4. Cell imaging

By analogy to the earlier development of antibody-based methods for cell imaging, aptamers have also enabled numerous cellular imaging applications, especially for imaging cancers [43]. Following are four recently reported applications for imaging cancer cells, three involving aptamers targeting cell surface glycoprotein receptors (sections 4.1 and 4.3), and then an example of dead-cell imaging (4.4), since dead vs. live cell-status is an important technical aspect of cellular imaging or detection that is sometimes overlooked.

4.1. Magnetic resonance imaging

The transmembrane glycoprotein mucin 1 (MUC1) is aberrantly glycosylated and overexpressed in a variety of epithelial cancers, and plays a crucial role in progression of the disease [44]. Tumor-associated MUC1 differs from the MUC1 expressed in normal cells with regard to its biochemical features, cellular distribution, and function. In cancer cells, MUC1 participates in intracellular signal transduction pathways and regulates the expression of its target genes at both the transcriptional and post-transcriptional levels. The structural and functional differences that exist between normal and tumor-associated MUC1, and advances in the use of MUC1 as a biomarker and therapeutic target for cancer, have been reviewed [44].

Zou et al. [45] explored the ability of magnetic resonance imaging (MRI) using MUC1-modified superparamagnetic iron oxide nanoparticle (SPION)-targeting of human pancreatic cancer (PC), the third leading cause of cancer deaths, and which is difficult to diagnose, for anatomical and other reasons, and is thus in need of early detection by non-invasive procedures such as MRI. The MUC1 target-directed aptamer was prepared through MUC1 conjugation to SPIONs (63 nm). BxPC-3 cells, which are a human PC cell line used in the study of pancreatic adenocarcinomas and treatments thereof, were employed in this investigation. BxPC-3 cells were cultured with MUC1-SPION and SPION under various conditions, and observed using Prussian blue staining, which is a common histopathology stain used by pathologists to detect the presence of iron in biopsy specimens. Cytotoxicity was assayed by the conventional MTS assay, a colorimetric method for sensitive quantification of viable cells in cell proliferation assays, and a nude mouse model of PC was established to investigate MUC1-SPION in vivo. MRI was performed to determine the intensity of the signal of the transplanted tumor, while immunohistochemistry and Western blot analyses were performed to detect the expression of MUC1 in tumor biopsies. Importantly, MUC1-SPIONs could significantly reduce MRI T_2-signal strength [46] and were nontoxic in vitro. In vivo MUC1-SPIONs selectively accumulated in PC tumors in the nude mice model, thus indicating the possible utility for early in vivo imaging of PC in humans.

4.2. Gold nanoparticles

The epithelial cell adhesion molecule (EpCAM) is a transmembrane glycoprotein that was originally identified as a marker for carcinoma, by its high expression on rapidly proliferating tumors of epithelial origin [47]. Telomeres, repetitive (TTAGGG) DNA–protein complexes at the ends of chromosomes, are crucial for the survival of cancer cells, and are maintained by an enzyme called telomerase (TE) in the vast majority of tumors. Although EpCAM has been previously used as an aptamer target for drug delivery and imaging, Guo et al. [48] recently reported a novel dual-aptamer approach for simultaneously imaging cells for both EpCAM and TE. In brief, they designed a ratiometric surface-enhanced Raman scattering (SERS) detection method to achieve high accuracy and sensitivity for the detection of TE and EpCAM in living cells using the DNA-guided, self-assembled tetrahedron structure (see 2020 review [49]) depicted in Fig. 6. This gold nanoparticle (AuNP) tetrahedron probe was comprised of three 15-nm AuNPs and two 30-nm AuNPs. The two 30-nm AuNPs were modified with SERS tags 4-nitrothiophenol (NTP) (blue pyramids) or 4-methoxybenzylmercaptan (MATT) (magenta stars), and were linked with a fluorescent Cy5.5 (red
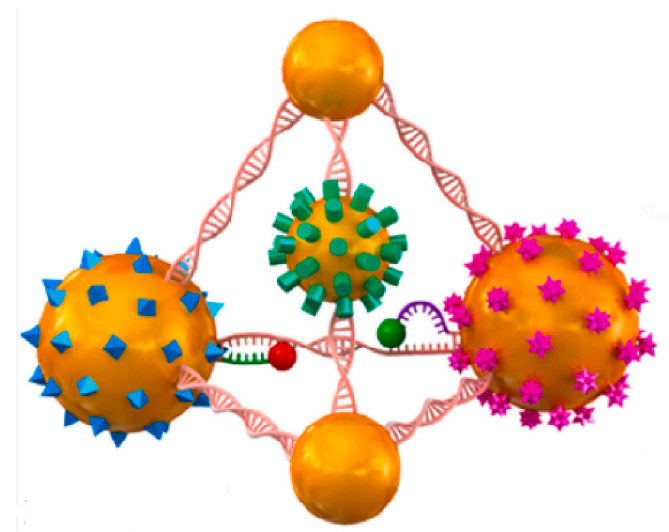
Fig. 6. Schematic depiction of a tetrahedron probe self-assembled from gold nanoparticles bonded to DNA oligonucleotide linkers, aptamers, and surface-enhanced Raman scattering tags for detection, as described in the text. Taken from Guo et al. [48] Anal. Chem. 2020, 92, 2, 2310–2315 with permission. Copyright © 2020, American Chemical Society. (For interpretation of the references to color in this figure legend, the reader is referred to the Web version of this article.)

dot)-labeled TE aptamer or a fluorescent TAMRA (green dot)-labeled EpCAM aptamer, respectively. In addition, one of the 15-nm AuNPs was SERS-tagged with 4-aminothiophenol (4-ATP) (green rods) as an internal reference.

In the presence of EpCAM or TE target, the dissociation of the corresponding AuNPs resulted in decreased SERS signals. Also, the ratios of Raman intensity for TE and EpCAM, compared with the internal reference, were shown to quantify the level of TE and EpCAM, respectively. The linear range of TE and EpCAM in the HeLa cancer cell line was 0.7×10^{-12} to 37×10^{-12} IU and 1.24–75.48 pg/mL, respectively, with a LOD of 7.6×10^{-16} IU and 0.53 pg/mL, respectively, consistent with the results of Raman confocal imaging. Based on the results of this study, it was concluded than the tetrahedron probe-system provides a reliable and ultrasensitive strategy for the in situ dual detection of biomarkers and a new method for SERS-based early diagnosis of cancer.

4.3. In silico aptamer selection

In contrast to the usual procedure of obtaining an EpCAM-specific aptamer by application of a selection process, such as cell-SELEX (e.g. [50]), Bell et al. [51] investigated selection in silico, which they say is highly sought after to facilitate virtual screening and increased understanding of important nucleic acid–protein interactions. In silico selection can also be a valuable adjunct for facilitating selection of a desired aptamer in the lab or optimization of sequence, and adding post-selection modifications to increase binding to target. As proof-of-principle, these researchers developed an in silico method that first predicted EpCAM aptamer binding modes and then optimized these interactions for two EpCAM aptamers with molecular dynamics simulations, docking, and free-energy calculations. Isothermal titration calorimetry experiments further confirmed that the EpCAM aptamers indeed exhibit enhanced affinity over a previously studied (e.g. [52]) nanomolar-binding aptamer, termed Ep23. Moreover, these in silico studies led Bell et al. [51] to conclude that Ep23 and the de novo designed aptamers primarily bind to EpCAM dimers (and not monomers, as hypothesized in previous published works), thus suggesting a paradigm for developing EpCAM-targeted therapies.

4.4. Dead cells

Dead cells always accompany live cells in vitro and in vivo. It is important to distinguish dead cells from live cells in various biological studies. Currently, the probes for dead cells are mainly nucleic acid-intercalators, most of which have low affinity and potential toxicity to live cells. To address this problem, Shen et al. [53] developed a novel aptameric probe (Ch4-1) that binds cell nuclei with high affinity (Kd = 6.65 nM). Ch4-1 was generated by a cell-SELEX process, and was shown to target nucleoproteins in cell nuclei. According to these researchers, this negatively charged oligonucleotide cannot penetrate the integrated cell membrane; therefore, it only binds to dead cells rather than live cells. Compared with traditional DNA-targeting nuclear dyes, Ch4-1 possesses a high affinity for the nucleus, does not exhibit toxicity to live cells, and can be easily labeled with different fluorescent dyes. It was demonstrated to serve as a probe for distinguishing dead cells from live cells using an apoptosis assay, and was also used for nuclear staining of tissue sections.

An interesting and challenging variant of dead-cell imaging or analysis deals with viable but non-culturable (VBNC) cells. According to a review by Ramamurthy et al. [54], many species of bacteria, under stress, enter into a starvation mode of metabolism or VBNC state, including several human pathogenic bacteria. These VBNC bacteria cannot be grown using conventional culture media, although they continue to retain their viability and can become virulent. One such pathogen is *Vibrio vulnificus*, which is a ubiquitous marine bacterium that can cause rapid and deadly infection; however, traditional culture-based methods are unable to detect VBNC *V. vulnificus* cells. In

2020, Liu et al. [55] reported the use of whole bacteria-SELEX to isolate aptamers specific for simultaneously binding to both live and VBNC *V. vulnificus*. One truncated version, which had a Kd of 11 nM, was used for confocal fluorescence microscopic imaging and enumeration by flow cytometry, exhibiting a linear range is 10^2 to 5×10^5 CFU/mL and a LOD of 30 CFU/mL.

5. Imaging RNA

The ability to image specific molecular targets in living cells opens exciting new avenues of research for elucidating the complexities of the genesis, spatial trafficking, decay, and temporal aspects of intracellular constituents. Chief among these intracellular molecules are various types of RNA, especially messenger RNA (mRNA) and microRNA (miRNA), because of their direct involvement in gene expression and regulation thereof, respectively. This section provides a brief introduction to how fluorogenic aptamers have been developed for imaging specific RNA of interest, and then gives very recent examples for mRNA (section 5.1) and miRNA (section 5.2).

In 2011, the Jaffrey lab published a seminal paper [56] in *Science* demonstrating the generation of RNA aptamers that bind small-molecule fluorophores resembling the fluorophore moiety in green fluorescent protein (GFP) to "create a palette that spans the visible spectrum" for use in imaging RNAs in living cells. As proof-of-principle, an RNA aptamer (24–2, Fig. 7)-fluorophore [3,5-difluoro-4-hydroxybenzylidene imidazo-linone (DFHBI)] complex, termed Spinach, which emits a green fluorescence comparable in brightness with GFP, was used to image RNA in living mammalian cells. For example, Spinach was fused to the 3′ end of 5 S, a small noncoding RNA transcribed by RNA polymerase III that associates with the large ribosomal subunit, and was transfected into human embryonic kidney cells. The 3′ end of 5 S is solvent exposed, and addition of short sequences to the 3' end does not affect 5 S localization. 5 S-Spinach fluorescence was detected throughout cells with a distribution similar to that of endogenous 5 S in the same cell type. Since 2011, this paper has been cited more than 850 times.

5.1. Imaging mRNA

Wirth et al. [57] recently noted that aptamer/ligand pairs emitting in the far-red and near-infrared (NIR) regions are still rare. They therefore developed a light-up RNA aptamer that binds silicon rhodamines (SiRs). SiRs are photostable, NIR-emitting fluorophores that change their open-closed equilibrium between the noncolored spirolactone and the fluorescent zwitterion in response to their environment (Fig. 8). This property is responsible for their high cell permeability and fluorogenic behavior. Aptamers binding to SiR were selected in vitro from a combinatorial RNA library that was comprised of a central stable-stem-loop (SSL) region flanked by random sequences (N) having terminal forward (F) and reverse (R) primer sequences (5′ $F_{19}-N_{26}-SSL_{12}-N_{26}-P_{20}$ 3') to bias selection of a three-way junction motif (Fig. 8). Subsequent sequencing, bioinformatic analysis, truncation, and mutational studies revealed a three-way junction motif comprising a 50-nucleotide minimal aptamer, SiRA, that binds with nanomolar affinity to the target SiR.

Additionally, SiRA binds structurally related rhodamines and carborhodamines, which makes it a versatile tool spanning the far-red region of the spectrum. Photophysical characterization showed that SiRA is remarkably resistant to photobleaching and constitutes the brightest far-red light-up aptamer system known to date owing to its favorable features: a fluorescence quantum yield (Φ)of 0.98 and an extinction coefficient (ε) of 86,000 M(-1) cm (-1). In a proof-of-principle study, these researchers employed the SiRA system to visualize the expression of mRNA in live bacteria in no-wash, quencher-free, live-cell imaging experiments. Furthermore, they successfully applied the SiRA system in the first light-up aptamer application of live-cell super-resolution microscopy (SRM) [58] images of aptamer-based, fluorescently labeled
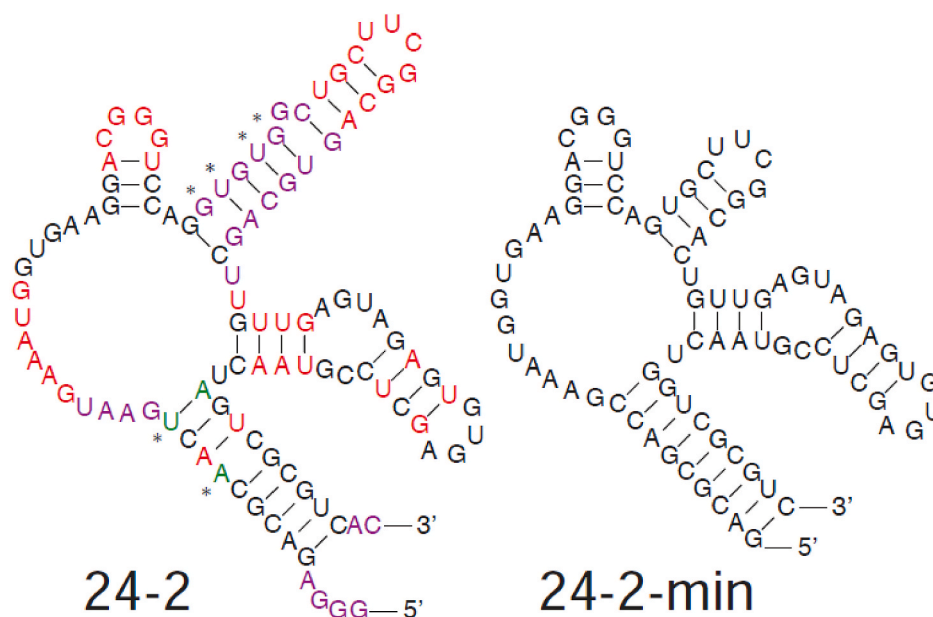
Fig. 7. RNA structure 24-2 shown as predicted by Mfold web-based software. Structural prediction was used to generate 24–2 DNA templates in which several bases at a time were removed from 5' and 3' ends. These truncated DNAs were in vitro transcribed into RNA and assayed for fluorescence. Bases that could be removed without significant loss in fluorescence are indicated in purple. Next, A-U, G-U and any mismatched base pairs were mutated to G-C base pairs and tested for their effect on 24–2 fluorescence. G-C mutations that reduced 24–2 fluorescence are indicated in red, those which had no effect are indicated by asterisk (*) and those which increased the fluorescence of 24-2 are indicated in green. The hairpin loop motifs CGGG and UUCG were swapped with the sequence UUCG or GAAA, respectively. Both swaps resulted in significantly reduced fluorescence signal suggesting that they are important for DFHBI binding. The final truncated 24-2 sequence, 24-2-min, is shown and exhibits ~95% of full-length 24–2 fluorescence. Taken from Paige et al. [56] Nat. Methods 2019, 16, 9, 862–865 with permission. Copyright © 2011 American Association for the Advancement of Science. (For interpretation of the references to color in this figure legend, the reader is referred to the Web version of this article.)
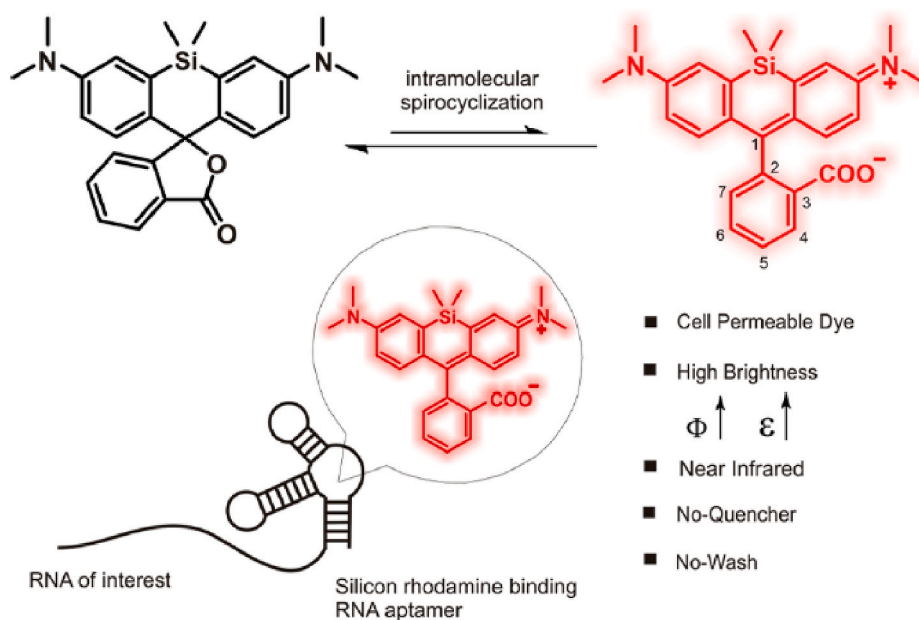

Fig. 8. General RNA labeling strategy using a SiR-binding aptamer. Top: Environment-dependent intramolecular spirocyclization of silicon rhodamines (SiRs). Bottom: The fluorescence increases upon binding of the aptamer to the SiR fluorophore, allowing visualization of the target RNA using fluorescence microscopy. Taken from Wirth et al. [57] J. Am. Chem. Soc. 2019, 141, 18, 7562–7571 with permission. Copyright © 2019 American Chemical Society. (For interpretation of the references to color in this figure legend, the reader is referred to the Web version of this article.)

mRNA in live cells. It was stated that, although this work was limited to prokaryotic systems, the application of SiRA to mammalian cells is currently under investigation, and that, to image RNAs of low abundance and to increase the sensitivity of the system, a large number of tandem repeats of SiRA can be genetically fused to the RNA of interest.

Notwithstanding the just mentioned (and other not cited) examples of fluorogenic dyes for aptamer-mediated imaging of mRNAs in live cells, Wu et al. [59] state that there are not many fluorogenic dyes that meet the criteria required for use of fluorogenic aptamers in live cells, and that most dyes show nonspecific fluorescence activation by cellular lipids or DNA. Another problem, they say, is that the fluorogenic dyes are not genetically encoded and therefore need to be added exogenously for RNA imaging, and that a genetically encoded conditionally fluorescent dye would therefore simplify the use of fluorogenic RNA aptamers.

While fluorescent proteins as such dyes are attractive because a diverse array of spectrally distinct proteins have been described, these proteins are constitutively fluorescent. To make them dependent on RNA, Wu et al. [59] considered making them rapidly degraded in cells except when bound by a specific RNA aptamer. In this way, fluorescence would be selectively associated with RNA-protein complexes, and not with unbound fluorescent protein. This would be functionally equivalent to RNA-induced fluorescence of small molecule dyes.

Proof-of-principle for this novel strategy was achieved by fusing a constitutively fluorescent protein (CFP), such as mNeonGreen, with tDeg, a bifunctional peptide that consists of the Tat peptide, which is capable of binding to an RNA aptamer, termed Pepper, and the previously described C-terminal Arg-Arg-Arg-Gly degron [60]. When fused to a CFP, tDeg causes protein degradation and loss of fluorescence.

However, the CFP destabilization function of tDeg is blocked when it binds to the Pepper RNA aptamer. To image β-actin mRNA localization in response to arsenite stress, Wu et al. [59] constructed a β-actin mRNA reporter containing a 3' UTR Pepper mRNA tag. Cells co-expressing this β-actin mRNA-Pepper construct and (mNeonGreen)₄-tDeg were imaged before and 45 min after arsenite (500 μM) treatment to induce stress granules. They observed individual mRNA transcripts that rapidly accumulated to form stress granules.

5.2. Imaging miRNA

MiRNAs are a large family of short (~23 nucleotides), noncoding RNAs that play a critical role in posttranscriptional regulation of gene expression [61]. Moreover, aberrant miRNA expression is associated with a wide range of human diseases, including cancer. Consequently, significant efforts have been made to image miRNA expression in living cells and organisms, for both basic research and early disease detection. Current strategies for imaging endogenous miRNAs mostly rely on the use of hybridization-based probes (e.g. signal-amplifying ribozymes [62]), all of which are composed of nucleic acids. Notwithstanding this utility for imaging miRNA in living cells, Zhong and Sczepanski [63] point out that, nucleic acid-based probes still suffer from two key limitations when applied to biological environments: rapid nuclease degradation and unintended hybridization with non-target nucleic acid macromolecules. In principle, they reason, such disadvantages associated with the use of nucleic acids in live cells can be overcome by simply inverting the stereochemistry of the sugar backbone to take advantage of the known resistance to nucleases of L-DNA and L-RNA, which are synthetic enantiomers (chiral mirror images) of natural D-nucleotides, and the inability of forming stable heterochiral (L/D) duplexes (reviewed in [64]).

To leverage these advantageous properties of L chirality in the context of miRNA imaging, Zhong and Sczepanski [63] utilized peptide nucleic acids (PNAs), which have no inherent chirality. As a result, PNA hybridizes to both DNA and RNA irrespective of D or L stereochemistry. As depicted in Fig. 9, the sensor consists of a duplex between an achiral PNA strand (green) and a fluorogenic L-RNA aptamer (blue), termed L-Mango. The L-Mango aptamer was chosen due to its high binding affinity toward its target dye, thiazole orange (TO), bright fluorescent signal, and small size relative to other reported fluorogenic aptamers (e. g., Spinach and Broccoli) [65]. Importantly, the TO dye is achiral, implying that it can be bound and activated by both D- and L-versions of the Mango aptamer. Critical intramolecular folding is blocked by the bound PNA strand. However, D-MicroRNA can cause heterochiral strand displacement to form a D-MicroRNA/PNA product (waste in Fig. 9) and thus allow L-Mango to undergo intramolecular folding, bind TO, and thereby induce fluorescence for detection. This initial sensor system was optimized for detection of miRNA-155, which is a prototypical oncogenic miRNA associated with the development and invasiveness of various types of malignancies.
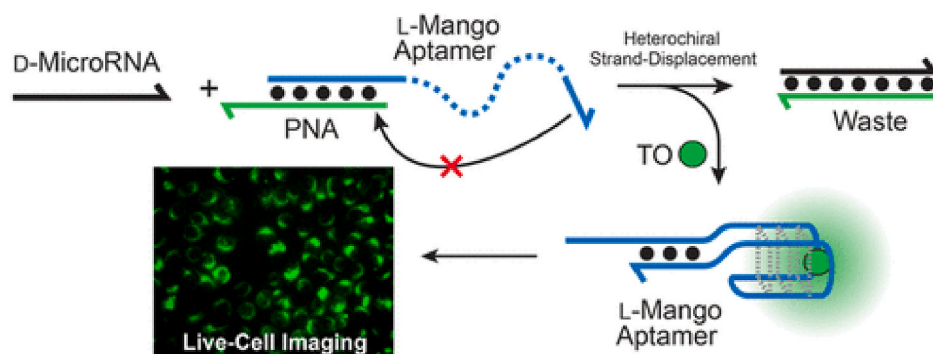
Rather than relying on traditional transfection reagents (e.g., Lipofectamine) to deliver this probe into cells, which can have adverse effects on cell viability, these researchers instead employed a well-known self-delivering strategy based on conjugation of cholesterol, in this instance to the 5' end of the L-Mango aptamer via a PEG linker construct. To test the ability of the self-delivering sensor to image miRNA-155 expression in living cells, an engineered HeLa cancer cell line stably over-expressing miRNA-155 (HeLa155, >200-fold over-expression relative to wild-type HeLa cells) was used. As shown in Fig. 9, the L-Mango/TO fluorescence signal was clearly evident in these cells, and was notably brighter compared to wild-type HeLa cells (see [63]). Unfortunately, treatment of wild-type HeLa cells with TO alone resulted in a fluorescence signal that was nearly equivalent to the same cells treated with the self-delivering L-Mango aptamer in the presence of TO, thus indicating that the TO dye itself causes background fluorescence in the absence of miRNA-155 expression. Zhong and Sczepanski [63] concluded that, although this was the first time L-oligonucleotides have been interfaced with a living system, it will be important to further optimize this imaging approach, possibly through the use of alternative dyes or aptamer−dye pairs, in order to increase the sensitivity of the sensor for detection for low copy-number RNAs in living cells.

6. Cell capture

Pioneering work on aptamer-based cell capture using microfluidics was independently published in 2009 by Tan and collaborators [66] and the Soper lab [67]. The Tan group developed an aptamer-based microfluidic device for enrichment, sorting, and detection of multiple types of cancer cells, which can be used to detect cancers at early stages, diagnose metastatic relapse, stratify patients for therapeutic purposes, monitor response to drugs and therapies, and track tumor progression. Similar utility was demonstrated by the Soper lab with peripheral blood that contained prostate tumor cells which over-express a prostate specific membrane antigen. During 2009–April 2020, Tan and collaborators [66] has been cited ~270 times, and the Soper lab [67] publication has been cited ~210 times.

6.1. Circulating tumor cells

"Liquid biopsies" involving analyses of circulating tumor cells (CTCs) and circulating cell-free tumor DNA (cfDNA a.k.a. ctDNA) in peripheral blood have received widespread attention because of the clinical implications for non-invasive sampling and early detection of cancers, as reviewed elsewhere [68] and updated in April 2020 for two clinical studies [69] of cfDNA. Studies of cfDNA in peripheral blood using deep sequencing by Shedure and collaborators [70] have shown promise for non-invasive monitoring, and indicate identification of cfDNA bound to histones and transcription factors (TFs), the latter being much less abundant. High-throughput SELEX of aptamers for TFs has been reported by Ogawa and Biggin [71], but aptamer-specific enrichment of

Fig. 9. Design of a mirror-image fluorogenic aptamer sensor for detection of miRNA in live cells. Schematic illustration of the heterochiral strand-displacement sensor mechanism. Oligonucleotides are depicted as lines with the half arrow denoting the 3′ end (or C-terminus for PNA), and black dots indicating complementarity. D-MicroRNA (black), L-RNA (blue), PNA (green), and thiazole orange (TO). Taken from Zhong and Sczepanski [63] ACS Sens. 2019, 4, 3, 566–570 with permission. Copyright © 2019, American Chemical Society. (For interpretation of the references to color in this figure legend, the reader is referred to the Web version of this article.)

TF-bound cfDNA appears to be an unexplored opportunity. By contrast, there has been considerable effort aimed at aptamer-based capture of CTCs. Indeed, Wu et al. [72] published a review in 2019 of progress in aptamer-based microfluidics for isolation, release and analysis of CTCs.

Notwithstanding the achievements using aptamer-based capture of CTCs discussed in Wu et al. [72], Song et al. [73] more recently stated that "the issue of compromised binding affinities and stabilities in real samples hinders its wide application". Consequently, and said to be "inspired by the high efficiency of the prey mechanism of the octopus", these researchers engineered a deterministic lateral displacement [74] (DLD)-patterned microfluidic chip modified with multivalent aptamer-functionalized nanospheres to enhance capture efficiency. Briefly, citrate-capped AuNPs (16 nm) were prepared using literature protocols, and a previously reported [75] EpCAM-binding aptamer, termed SLY3C, having three stem-loops was attached to the AuNPs via a 5′-thiol-C6 linker. A 5′-biotin on SLY3C served as a capture "handle" by streptavidin attached to the surface of the chip's pillars. The number of aptamer strands attached to each AuNP was determined to be ~250, and it was reasoned that, similar to multivalent trailing tentacles used by an octopus for hunting, these aptamers could exert cooperativity and lead to stronger binding. It was further reasoned that binding of a number of these SLY3C-decorated AuNPs to a cancer cell would increase its effective size, relative to blood cells or other types of background cells, and thus facilitate separation by the DLD-patterned chip. Measurement and optimization of capture efficiency were performed using three EpCAM$^+$ cell lines and one EpCAM$^-$ cell line. Glutathione was used to cleave the aptamer's thiol bond to gold under mild conditions and thus release the captured cells with 80% efficiency and 96% viability for analysis or culturing. For clinical evaluation of this method, blood samples from 3 healthy volunteers, 13 colorectal cancer (CRC) and 25 blinded samples of prostate disease were processed without any pretreatment. Four markers were used to classify and count (by FACS) cells as CTCs. In this manner, validated CTCs were successfully identified and enumerated by this aptamer-based Au NP system in all CRC and prostate cancer patients, while there were no CTCs in healthy and hyperplastic prostate donors.

A subsequent publication by Yang et al. [76] described a novel variant of SLYC3 that is catenated with intervening oligo-T spacers to give what is called a "multivalent network" of SLYC3 aptamers for more efficient, multivalent cooperative-capture of EpCAM$^+$ cancer cells. This network of concatenated aptamers was generated in situ by rolling circle amplification using a primer attached to a gold electrode by a thiol-gold bond. After capture, electrochemical detection is mediated by AuNPs decorated with anti-EpCAM antibodies. MCF-7 breast cancer cells were thus detected at an impressive LOD of only 5 cells/mL.

Cancer cell capture, detection and release were achieved in a much different manner by Ou et al. [77], who reported a novel sandwich-type "cytosensor" based on a DNA tetrahedron-linked dual-aptamer (reminiscent of that described in section 4.2) and a metal organic framework (MOF), which is a broad class of compounds consisting of metal ions or metal clusters coordinated with organic ligands to form one-, two-, or three-dimensional structures that are often porous. Applications of functional MOFs in biosensors have been reviewed in 2020 by Du et al. [78]. In the present instance, the tetrahedron DNA nanostructures comprised of linked aptamers to both AS1411 (section 2.) and MUC1 (section 4.) were immobilized on a gold electrode surface as bio-recognition elements to capture MCF-7 cancer cells and improve the density and orientation of surface nanoprobes. The MOF, termed PCN-224, which is a zirconium-based porphyrine-containing structure that can be metalated [79], was homogeneously decorated by platinum nanoparticles and further modified by a known G-quadruplex-hemin horseradish peroxidase-mimicking DNAzyme [80]. The fabricated nanoprobes catalyze the oxidation of hydroquinone with hydrogen peroxide for amplifying the electrochemical signal. The results indicated that the linear response of the aptamer-mediated cytosensor ranged from 20 to 1×10^7 cells/mL and the detection limit was 6 cells/mL.

Finally, these researchers performed an electrochemical reductive desorption to break thiol-gold bonds and release all compounds on the electrode surface for analyzing the viability of collected cells and regenerating the cytosensor. It was suggested that this method can be extended to other types of cancer cells by using other cancer cell type-specific aptamers, and could be by applied to point-of-care (section 10.) cancer diagnosis.

7. Bi-specific aptamers

In 2002, James and collaborators [81] reported the first bi-specific (also spelled bispecific) aptamers by first selecting for 2′-fluoro-substituted RNA aptamers that bind to streptavidin (SA) with an affinity of ~7 nM, which was not prevented by prior saturation of SA with biotin, its natural ligand. In order to provide a general method for the exploitation of these aptamers, these researchers then produced derivatives that can simultaneously bind SA and a second protein, by fusing to the RNA elements CopT or CopA, which are discussed elsewhere [82]. In parallel, they produced derivatives of CD4-binding aptamers fused to the complementary CopA or CopT elements. When mixed, these two chimeric constructs rapidly hybridized, by virtue of CopA-CopT complementarity, to form stable, bi-specific aptamers, which James and collaborators [81] called "adaptamers". It was then showed that the bi-specific CD4-SA-binding aptamer can be used to capture CD4 onto a SA-derivatized surface, thus illustrating potential general utility.

Published literature using the term bi-specific aptamers or adaptamer was absent until several papers by other researchers appeared in 2011 [83–85], which have been followed by 20 additional studies, 7 of which appeared in 2019. During this adoption period, bi-specificity has been expanded to include aptamer-antibody constructs. Following are several examples of bi-specific aptamers selected from the 2019 literature, two involving therapeutics and one directed toward imaging.

7.1. Therapeutics

Although numerous monoclonal antibodies have been approved by the Food and Drug Administration for the treatment of a wide variety of disease, including cancer, clinical trials of candidate aptamer drugs for various indications have not yet met with success, as reviewed elsewhere [28]. Among the reasons for this lack of success in the clinic is inadequate potency or specificity or both, which might be remedied by employing bi-specificity strategies.

For example, Passariello et al. [86] investigated two novel bi-specific aptamer conjugates, consisting of an anti-EGFR (section 2.) aptamer linked with either an anti-ErbB-2 compact antibody or with an immunomodulatory (anti-PD-L1) antibody, which were easily and rapidly obtained. Using well-known [87] conjugation reagents, 2′-fluoro pyrimidine RNA aptamers, termed CL4, as corresponding versions containing a C6-NH$_2$ or a biotin, were functionalized with an aromatic aldehyde group (formylbenzamide, 4FB) by reaction with an amine-reactive NHS ester. In the second step, Erb-hcAb or 10_12 antibody was modified with flag-tagged HyNic-functional groups by incubating the antibody with a hydrazine-containing S-HyNic reagent. Then, 4FB-oligonucleotide was incubated with HyNic-modified antibody to allow for spontaneous aldehyde-hydrazine conjugation to give the two bi-specific conjugate structures depicted in Fig. 10.

These novel bi-specific aptamer-antibody conjugates retain the targeting ability of the parental moieties and acquire a more potent cancer cell-killing activity by combining their inhibitory properties. Furthermore, the conjugation of the anti-EGFR aptamer with the immunomodulatory antibody allowed for the efficient redirection and activation of T cells against cancer cells, thus dramatically enhancing the cytotoxicity of the two conjugated partners. It was suggested that these bi-specific antibody-aptamer conjugates could have optimal biological features for therapeutic applications, such as increased specificity for tumor cells expressing both targets, and improved pharmacokinetic and
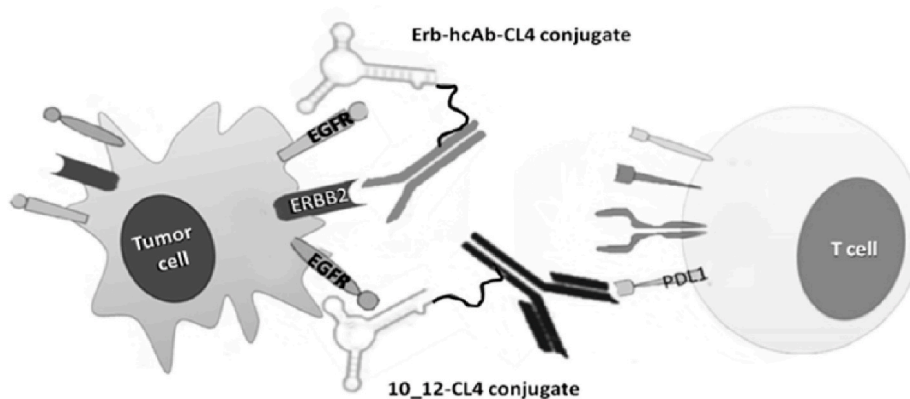
Fig. 10. Schematic depictions of Erb-hcAb-CL4 (grey) or 10_12-CL4 (black) conjugates, generated by the fusion of CL4 amino-oligonucleotide (anti-EGFR aptamer) with the Fc region of Erb-hcAb (anti-ErbB2 compact antibody) or 10_12 (anti-PD-L1 monoclonal antibody). Taken from M. Passariello et al. [86] Cancers (Basel) 2019, 11, 9, 1268 with permission. Open Access.

pharmacodynamic properties due to the combined advantages of the aptamer and antibody.

In a conceptually related study, Li et al. [88] described a promising strategy for cancer immunotherapy that employed a bi-specific aptamer that can bind with both tumor cell markers and immunocytes for recruitment of lymphocytes to tumor sites and enhancement of anti-cancer immune reactions. MUC1 (section 4.) is a tumor marker over-expressed in almost all adenocarcinomas, making it a potentially important therapeutic target. CD16 is expressed in several types of immunocytes, including natural killer (NK) cells, gamma delta-T cells, monocytes, and macrophages. Therefore, these researchers targeted both MUC1 and CD16, but in a novel way. Briefly, they used a bivalent bi-specific aptamer, termed BBiApt, that had two MUC1 aptamers and two CD16 aptamers linked together by three 60-nucleotide DNA spacers (S_{60}) in the following 5′ to 3′ order: 5′ MUC1- S_{60}-CD16$^-$ S_{60}-MUC1- S_{60}-CD16 3′. This quadrivalent construct could be expected to exhibit cooperativity and, hence, stronger binding. Indeed, compared with monovalent MUC1 or CD16 aptamers, BBiApt showed more potent avidity to both MUC1-positive tumor cells and CD16-positive immuno-cytes. Competition experiments indicated that BBiApt and monovalent aptamers bound to the same sites on the target cells. Moreover, BBiApt recruited more CD16-positive immunocytes around MUC1-positive tumor cells and enhanced the immune cytotoxicity against the tumor cells in vitro, thus providing promising results to support further development or extension to other aptamers and tumor targets.

7.2. Imaging

In fluorescently activatable aptamer probes (AAPs a.k.a. "light-up" probes) the normally quenched fluorescence can be restored by unquenching via target-activated conformational changes of AAPs. In comparison to "always-on" probes with constant signals, AAPs can provide suppressed background levels, thus affording rapid and contrast-enhanced imaging for precise and sensitive tumor diagnosis. However, according to Shi et al. [89], reported shape-switching-dependent AAPs are still challenged by unsatisfactory noise suppression, poor stability, and sophisticated sequence design.

Dysregulated pH, resulting from aerobic glycolysis of cancer cells, has been extensively studied. Unlike cell surface receptors that vary according to cancer cell types, decreased extracellular pH is a ubiquitous characteristic of solid tumors, thus providing a potential target stimulus for designing simple and generally activatable probes. Shi et al. [89] envisioned fusion of pH-responsive elements and aptamers as bi-specific molecular probes for tumor imaging that are an improvement over a previously reported split i-motif [90] construct that had high back-ground and false positives. As an alternative pH-sensitive element they

utilized 3,9-bis(3-aminopropyl)-2,4,8,10-tetraoxaspiro [5.5]undecane (ATU) [91]. As proof-of-concept, an aptamer termed S6, which was selected against human lung cancer A549 cells by cell-SELEX, was 5′-carboxylated and Cy5-labeled (COOH-Cy5-S6) and linked to ATU using sulfo-NHS. The resultant intermediate was then reacted with NHS-BHQ2 quencher to produce the final product, termed pH-AAP. At neutral pH, in normal tissues or blood, the ATU linker remains intact, which keeps Cy5 in close proximity to BHQ2, leading to the quenched fluorescence of pH-AAP. Once it reaches the target area, pH-AAP can accumulate on the tumor cell surface on the basis of the specific binding of aptamers to target receptors, where due to lower pH of tumor tissues, acid-catalyzed hydrolysis of acetal groups can occur, thus leading to unquenching and Cy5 fluorescence.

In vivo bi-specific tumor imaging was performed using the pH-AAP strategy. After intratumoral injection with the corresponding test probes, time-lapse fluorescence imaging was conducted for nude mice bearing different tumors. As shown in Fig. 11, an obvious fluorescence recovery was observed in A549 tumor, targeted by the S6 aptamer, 2 min post-injection of pH-AAP, due to acidic-microenvironment-triggered hydrolysis of ATU linkers. As a result of continuous activa-tion and specific accumulation of pH-AAP, fluorescent signals in the A549 tumor gradually enhanced and reached the highest contrast at 120 min. With the slow clearance of probes by blood circulation, the fluo-rescence gradually faded, but clear tumor imaging was still seen at 300 min post-injection. In comparison, pH-ALP, an ATU-linked negative control, random-sequence probe showed very low fluorescence, as did pH-AAP-treated SMMC-7721 tumor derived from a human liver cancer cell line. It was concluded that this strategy might provide a new avenue for developing simple and universal molecular pH-AAPs with ultralow background and high specificity for cancer detection.

8. Protein detection

Detection of proteins using aptamers covers a broad range of appli-cations that have been addressed via a wide variety of formats. For the period 2019–April 2020, there are over 20 reports in PubMed having (protein AND detection) AND aptamer in the title. Following are several examples from this literature in early 2020 that illustrate how aptamer-protein binding has been used to develop devices applicable to medi-cally relevant cases that include point-of-care (section 10.). These ex-amples in sections 8.1-8.3 are inflammatory disease, neurodegenerative diseases, and breast cancer, respectively. But first, it should be noted that this account does not include SOMAmers (Slow Off-rate Modified Aptamers), which have hydrophobic aromatic side chains attached to the 5-position of uracil that create unique intramolecular motifs and make direct contacts with proteins. Importantly, SOMAmers engage
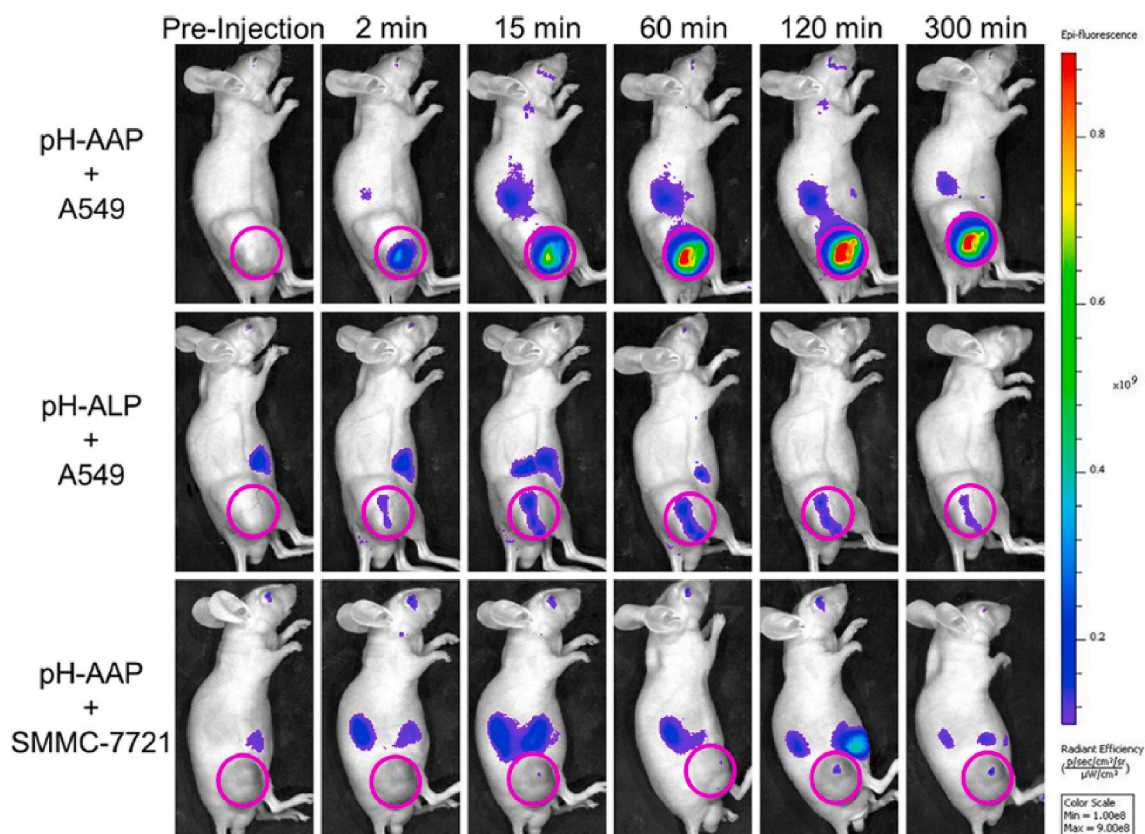
Fig. 11. In vivo fluorescence imaging of nude mice grafted with different tumors after intratumoral injection with different probes. The pink circles locate the tumor sites. Taken from Shi et al. [89] Anal. Chem. 2019, 91, 14, 9154–9160 with permission. Copyright © 2019 American Chemical Society. (For interpretation of the references to color in this figure legend, the reader is referred to the Web version of this article.)

their protein targets with surfaces that have significantly more hydrophobic character compared with conventional aptamers, thereby increasing the range of epitopes that are available for binding. These improvements have enabled building a collection of SOMAmers to over 3000 human proteins encompassing major families such as growth factors, cytokines, enzymes, hormones, and receptors, with additional SOMAmers aimed at pathogen and rodent proteins, as initially reviewed in 2014 by Gold and coworkers [92], and then others in 2017 [93]. SOMAmers represent a major advance in aptamer design as well as aptamer-based proteomics.

8.1. Inflammatory disease

C-reactive protein (CRP) is an evolutionarily highly conserved member of the pentraxin superfamily of proteins, and is widely used as a marker of inflammation, infection, and for risk stratification of cardiovascular events, as recently reviewed by McFadyen et al. [94]. A simple and fast colorimetric method for CRP detection that employs citrate-capped AuNPs (section 6.1) and a CRP-binding aptamer as sensing elements was reported by António et al. [95] in 2020. The aptamer was comprised of a G-rich single-stranded DNA (ssDNA) that adsorbs onto the surface of the AuNPs. In the presence of CRP, the ssDNA releases from the AuNPs surface to interact preferentially with the protein via G-quadruplexes (Fig. 4). The exposure of the unprotected AuNPs to buffer salts leads to aggregation and subsequent color change from wine-red to blue-purple that is readily seen by the naked eye. The AuNPs aggregation was monitored using UV–vis spectroscopy and the CRP concentration in samples could be correlated with the aggregation ratio (A_{670nm}/A_{520nm}). A linear sensing range of 0.89–20.7 μg/mL was found. The LOD was 1.2 μg/mL (8 nM), which is comparable to the typical clinical cutoff concentration in high-sensitivity CRP assays (1

μg/mL) and lower than the detection limit of nephelometric methods used in clinical practice. This method can provide a fast (5 min analysis time), simple, and sensitive approach to CRP detection, with negligible interference of serum albumin up to concentrations of 100 nM.

More recently, Minagawa et al. [96] have reported SELEX for human CRP using a pool of nucleobase-modified oligonucleotides comprised of uridine and adenine nucleotides linked to adenine and guanine nucleobases. These structurally novel constructs led to selection of a human CRP-specific aptamer having a Kd value of 6.2 pM, which reflects extraordinarily tight binding, and suggests the possibility of this aptamer being used for aptasensing of CRP with a significantly lower LOD than that mentioned above.

8.2. Neurodegenerative diseases

As discussed elsewhere [97], abnormal filaments consisting of a hyperphosphorylated microtubule-associated protein termed tau form in the brains of patients with Alzheimer's disease, Down's syndrome, and various dementing tauopathies. In Alzheimer's disease and Down's syndrome, the filaments have two characteristic morphologies referred to as paired helical and straight filaments, whereas in tauopathies, there is a wider range of morphologies. Using tau epitopes predisposed for phosphorylation, Teng et al. [98] in 2018 reported the identification of six distinct aptamers that bind to tau at two phosphorylatable epitopes (Thr-231 and Ser-202) and to full-length tau441 proteins with nanomolar affinity, noting possible use for detecting tau in biofluids.

The potential utility of tau-targeted aptamers was subsequently demonstrated in 2020 by Ziu et al. [99]. Their novel optical biosensor for tau441 protein was based on an aptamer-recognition probe and the biolayer interferometry [100] method for detection. A biotin-labeled aptamer for tau441 was attached to the streptavidin-coated surface of

a probe to provide real-time monitoring of tau441 protein in the nanomolar range, with a LOD of 6.7 nM in vitro. The tau441 protein is detected with high selectivity over other neurodegeneration biomarkers that include amyloid-β and α-synuclein. It was shown that this aptasensor allows for tau441 protein detection in a complex matrix such as fetal bovine serum, indicating its utility in other biological fluids for diagnostic applications. It was concluded that this optical method is simple, rapid and highly selective for point-of-care applications, which are critical for achieving the early and differential diagnosis of neurodegenerative diseases to guide treatments.

8.3. Breast cancer

According to a 2018 review by Perrier et al. [101], overexpression of epidermal growth factor receptor HER2, a transmembrane protein, is associated with an aggressive form of breast cancer and a poor clinical prognosis. Consequently, HER2 is considered to be an informative and actionable biomarker for monitoring breast cancer [102].

In a study reported in 2020 by Ranganathan et al. [103], two approaches for such monitoring were examined using HER2-binding aptamers and AuNPs. The first method used was a solution-based adsorption-desorption colorimetric approach wherein aptamers were adsorbed onto the AuNP surface in aggregates (Fig. 12). Upon the addition of recombinant HER2, HER2 binds specifically with its aptamer, dispersing the AuNPs. Addition of NaCl then induces the formation of AuNP aggregates, which leads to a color change from red to blue visible to the naked eye, and achieves an LOD of 10 nM. The second method used an adsorption-desorption colorimetric lateral flow assay (LFA) approach wherein the biotin-modified aptamers were adsorbed onto the AuNP surface in the absence of HER2. In the presence of HER2, HER2 specifically binds with its aptamer leading to release of the AuNPs. These solutions were applied to the LFA format and an LOD of 20 nM was achieved. Selectivity of the LFA format for HER2 was demonstrated using a scrambled-sequence aptamer as well as other proteins, including mammaglobin A, bovine serum albumin, thrombin, and ovalbumin.

For comparative purposes, these investigators discussed several electrochemical and ELISA-based HER2 biosensors that use different recognition materials, and have LODs from 0.07 to 0.7 nM, which are lower than the 10–20 nM LODs achieved by the present LFA format, whereas a more similar fluorometric assay using a HER2 aptamer has an LOD of 38 nM. Ranganathan et al. [103] stated that their LFA system has several advantages over electrochemical and ELISA-based HER2 biosensors. It is relatively fast, requiring only 30 min to perform, whereas electrochemical techniques require 2 h. The color-change is visible to the naked-eye making result interpretation easy for non-specialists. Also, it does not require expensive instruments, making it viable for point of care diagnosis. Their method was also said to be better than current clinical detection methods for overexpression of HER2 in breast cancer patients, such as immunohistochemistry (IHC) and fluorescence in situ hybridization (FISH). IHC is less reliable because it is influenced by a variety of analytical factors; FISH is expensive and requires instrumentation to detect time-sensitive fluorescent signals.

9. Food and water analysis

Global food and water safety issues have prompted the development of highly sensitive, specific, and fast analytical techniques for food and water analysis. The electrochemical aptamer-based detection platform is one of the more promising detection techniques because of its unique combination of advantages that renders these sensors ideal for detection of a wide range of target analytes, including those of concern for food and water safety, as reviewed by Li et al. [104]. The literature search used for this account indicated a preponderance of methodologies for detection of mainly heavy metal and other ions as pollutants. Selected ionic pollutants from that search include the 11 instances in section 9.1, with mercury receiving the most attention (5-of-11). That is followed by aptamer-based analysis of pathogens and pesticides in sections 9.2 and 9.3, respectively. Importantly, these various examples include demonstrations of analysis of contaminants in actual food and water samples.

9.1. Ionic pollutants

9.1.1. Mercury

Kiruba Daniel et al. [105] state that mercury (Hg) is one of the most acute toxic heavy metals at trace levels and its detection at parts per billion (ppb) in a low-cost, simple way remains challenging. They go on
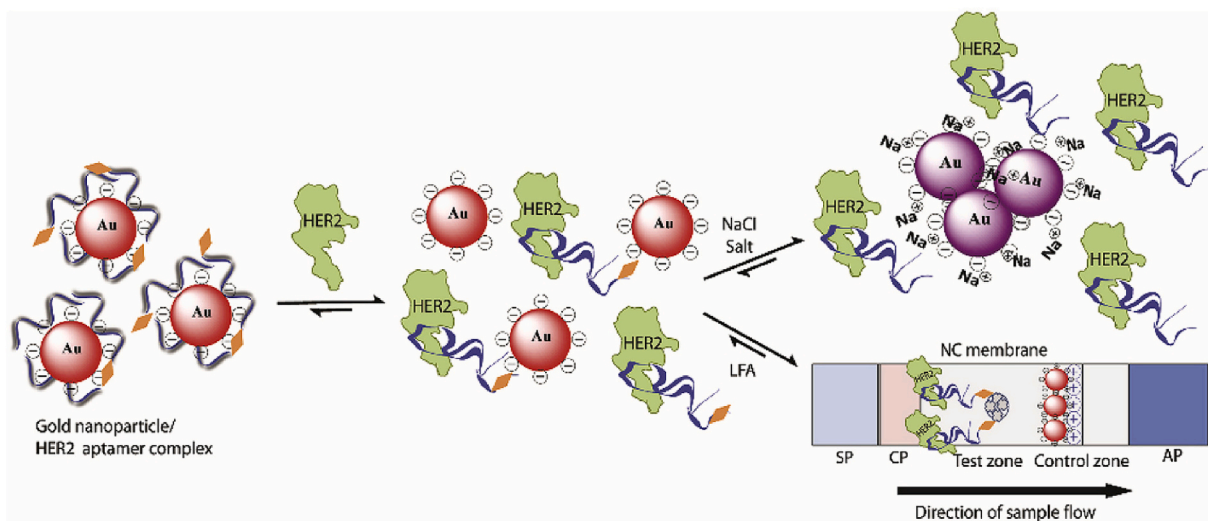

Fig. 12. Schematic illustration of the adsorption-desorption colorimetric LFA for HER2. Left: biotin (orange)-modified HER2 binding aptamers (grey) are adsorbed onto the AuNP surface (red) to form an aptamer/AuNP complex. Center: in the presence of HER2 (green), HER2 binds with its aptamer to form a HER2/aptamer/AuNP complex resulting in dispersion of the AuNPs. Right, top: in the presence of NaCl there is displacement of HER2/aptamer and visibly-detected aggregation of AuNPs (purple). Right, bottom: in the LFA format, the presence of HER2 leads to binding with its aptamer and dispersion of the AuNPs (red spheres). This leads to the absence of a red color in the test zone as the aptamer/HER2 complex binds to the streptavidin on the membrane. The control zone has a charged polymer that traps AuNPs non-specifically. Taken from Ranganathan et al. [103] Anal. Biochem. 2020, 588, 113,471 with permission. Copyright © 2019 Elsevier Inc. (For interpretation of the references to color in this figure legend, the reader is referred to the Web version of this article.)

to describe a handheld, low-cost electronic device for rapid, real-time fluorescence-based detection of mercuric ion (Hg^{2+}) using aptamer-templated zinc oxide (ZnO) QDs. Binding of Hg^{2+} with a single-stranded thymidine (T)-rich aptamer leads to the formation of a double-stranded structure bridged by T-Hg^{2+}-T moieties, and this acts as a template for the formation of ZnO QDs. With an increase in the concentration of Hg^{2+}, they observed an increase in duplex formation, leading to enhancement in the fluorescence. The LOD of the device is 0.1 ppb (0.5 nM), and experimental analysis has a linear range of detection between 0.1 and 10,000 ppb. The sensing was implemented as a prototype of a simple working electronic detection device.

An alternative detection scheme using the above-mentioned Hg^{2+}-driven formation of duplexed T-Hg^{2+}-T moieties was reported by Guo et al. [106], who devised an exciton energy transfer-based fluorescent sensor for the detection of Hg^{2+} through aptamer-programmed self-assembly of fluorescent cadmium-tellurium (CdTe) QDs. Basically, two versions of these QDs were prepared, each with self-complementary oligonucleotides having a stretch of three contiguous T nucleotides. Upon addition of increasing amounts of Hg^{2+}, there was formation of duplexed T-Hg^{2+}-T moieties, which brought the QDs into close proximity and thus led to fluorescence quenching, with an LOD of 3.3 nM.

Si et al. [107] reported electrochemical amplification for quantification of Hg^{2+} in water samples by anchoring an enzymatically extended aptamer. Similar to the above-mentioned two examples, this strategy is based on the Hg^{2+}-induced selective interaction of thymine mismatched pairs in a thymine-rich aptamer DNA to improve the specificity, while template-independent terminal deoxynucleotidyl transferase (TdT) extends the 3'-OH aptamer termini with repeated bases and increased the sensitivity. The introduction of Hg^{2+} blocks aptamer extension. This aptamer-TdT-based amplification sensor enabled the specific quantification of Hg^{2+} ion over a linear range of 2 pM–20 nM with an LOD of 0.1 pM.

In another variant of the above strategies, Abu-Ali et al. [108] reported the development of an electrochemical biosensor for high selectivity and rapid detection of Hg^{2+} (or Pb^{2+}) ions using aptamer probes labeled with ferrocene (or methylene blue) and thiol groups at their 5' and 3' termini, respectively. The strategy depicted in Fig. 13 relies on the principle that each type of aptamer could act as chelating agent for the analytes and undergo conformational changes that lead to changes in the electrochemical properties of the aptamers containing the redox label. The anti-Hg^{2+} aptamer changes to a hairpin structure accommodating several Hg^{2+} ions due to T-Hg^{2+}-T interactions, while the anti-Pb^{2+} aptamer forms a G-quadruplex, accommodating Pb^{2+} ions due to G-Pb^{2+}-G interactions. In both cases, the redox labels come closer to the electrode surface and increase the electron transfer, i.e. electrochemical current. The detection of Hg^{2+} and Pb^{2+} ions in a wide range of concentrations as low as 0.5 nM (0.1 ppb) was achieved.
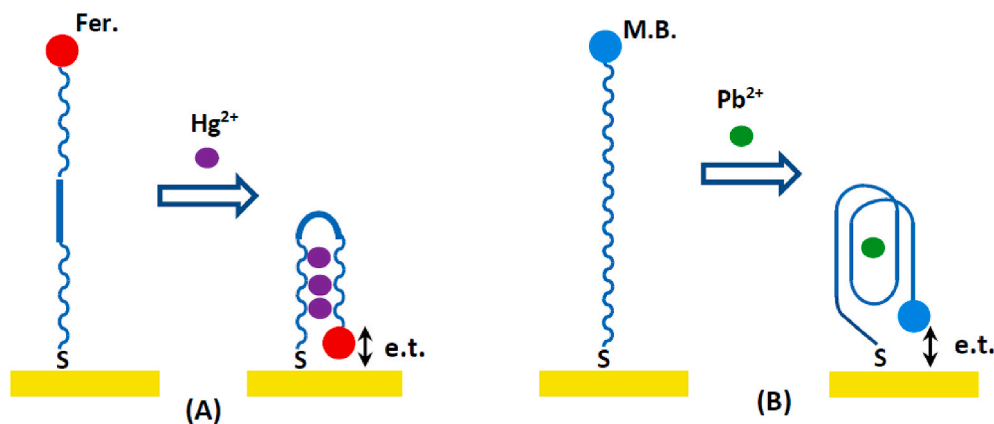
Berlina et al. [109] reported rapid visual detection of Hg^{2+} or Pb^{2+} in homogeneous solution using AuNPs conjugated with a T/G-rich aptamer. In presence of target ions, the modified AuNPs aggregate, thus resulting (after 20 min) in a change of the solution color from pink (for dispersed Au NPs) to blue (for aggregated Au NPs), formally analogous to that depicted in Fig. 12. Also, an amplification system for this assay was developed, based on the addition of 2-mercaptoethanol, which allowed a decrease in the LOD to 120 ng/mL for Pb^{2+} and 500 ng/mL for Hg^{2+} compared to 1 μg/mL and 4 μg/mL, respectively, for the method without amplification.

9.1.2. Lead

In addition to the above-mentioned sensors for Pb^{2+} reported by Abu-Ali et al. [108] and Berlina et al. [109], Yu et al. [110] reported a strategy for the "ultra-trace" level detection of Pb^{2+} based on a G-rich aptamer (5' GGTGGTGGTGGTTGTGGTGGTGGTGG 3') labeled with 5'-methylene blue, which is conceptually analogous to the Pb^{2+}-specific aptamer given in the caption for Fig. 12. In this case, the G-rich aptamer is simply absorbed onto the surface of an electrochemically reduced graphene oxide (ERGO) electrode via π-π electron interactions between the aptamer's nucleobases and the extensive π-electron system of graphene. As in Fig. 12, the presence of Pb^{2+} induces folding of the aptamer into a G-quadruplex structure; however, in this case, G-quadruplex formation results in detachment of the aptamer from the ERGO electrode, leading to a change in redox current of the methylene blue tag. Electrochemical measurements showed that the sensor had a linear range from 10^{-15} to 10^{-9} M and a remarkably low ("ultra-trace") LOD of 0.51 fM. Furthermore, the sensor had high selectivity for Pb^{2+} detection, as demonstrated by control experiments in the presence of various metal ions (Cd^{2+}, Co^{2+}, Ag^+, Cu^{2+}, Mg^{2+}, Ni^{2+}, Zn^{2+}, and Fe^{2+}), none of which resulted in a discernible voltammetric change.

9.1.3. Arsenic

In pioneering work reported in 2009, Kim et al. [111] used resin-bound phenylarsine oxide for SELEX of a DNA aptamer, termed Ars-3, to remove arsenic from groundwater. Surface plasmon resonance (SPR) revealed the Ars-3 aptamer had the highest affinity to arsenate [As(V)] and arsenite [As(III)] with Kd values of ~5 nM and ~7 nM, respectively, which were ~10^{-3} times lower than that for Co^{2+}, Mg^{2+}, Mn^{2+}, and Ni^{2+}. This publication has been frequently cited in related applications, and in 2019 Matsunaga et al. [112] reported development of a simple analytical method to determine arsenite using Apt-3 attached to AuNPs. In the absence of As(III) in a groundwater sample, the Apt-3/AuNPs give rise to a red colored solution. The presence of As (III) leads to detachment of Apt-3 from the AuNPs, which then aggregate and generate a purple colored solution. Conditions were optimized for NaCl concentration, incubation time (10 min) and buffer (pH = 7.3)

Fig. 13. Schematic depiction of electrochemical (electron transfer, e.t.) detection of heavy metal ions Hg^{2+} (**A**) and Pb^{2+} (**B**) using redox-labeled aptamers attached to gold surfaces. The aptamer for Hg^{2+} is 5'-ferrocene (Fer.)-TTCTTTCTTCCCCTTCTTTCTT-SH 3', and the aptamer for Pb^{2+} is 5'-methylene blue (M.B.)-CAACGGTTGGTGTGGTTGG-SH 3'. Taken from Abu-Ali et al. [108] Chemosensors 2019, 7, 2, 27 with permission. Open Access. (For interpretation of the references to color in this figure legend, the reader is referred to the Web version of this article.)

prior to determining a calibration plot, which was linear from 1 μM to 10 μM As(III) and had an LOD of 2 μM. Groundwater samples were simply filtered and subjected to treatment with a cation-exchange resin prior to determination of As(III).

In a much more sensitive variation of this method, Yadav et al. [113] reported the use of a glassy carbon electrode modified with silver and gold (Ag-Au) alloy NPs loaded with Apt-3 (or an analog thereof) and cyclic voltammetry. Captured As(III) ions undergo electrochemical reaction, thus producing a significant increase in the current. The activity curve is linear for As(III) concentrations of 0.36 nM–36 nM, and the detection limit is 0.12 nM.

9.1.4. Cadmium

Xu et al. [114] developed a highly selective and sensitive method for Cd^{2+} detection based on a Cd^{2+}-specific aptamer and AuNPs combined with colorimetric detection using a smartphone (section 10.). Based on Mfold calculations, it is proposed that Cd^{2+} binds to lone-pair electrons of nitrogen and oxygen in adjacent T and G nucleobases in the aptamer. The method utilizes an aptamer competitive binding assay with a cationic polymer polydiene dimethyl ammonium (PDDA) chloride solution. In the presence of Cd^{2+} the color of the AuNP solution changes from red to blue, in proportion to an increase in Cd^{2+} concentration. The color of the AuNP solution is photographed by an application downloaded on smartphone, and red and blue colors are determined as signal intensity for plotting a standard curve. The proposed method exhibited a linear range from 10 nM to 4 μM with a LOD of 10 nM. It was stated that this method has been successfully applied to test and quantify Cd^{2+} in water and rice samples, and that the results were in full agreement with those from the atomic absorption spectrometer. It was also suggested that this approach can be readily adapted to other analytes.

9.2. Pathogens

9.2.1. Pseudomonas aeruginosa

Pseudomonas is a group of bacteria that can cause various types of infections. *P. aeruginosa* is the most common disease-causing species, according to the U.S. Centers for Disease Control and Prevention (CDC). Serious infections from *P. aeruginosa* generally occur only in healthcare (nosocomial) settings, but people can also develop mild infections in other environments. Despite various advancements in biosensing, the rapid, accurate, and on-site detection of a bacterial pathogen is challenging due to the lack of appropriate diagnostic platforms. To address this unmet need, Das et al. [115] reported colorimetric and electrochemical aptamer-mediated detection of *P. aeruginosa* utilizing peroxidase-mimic activity of an AuNP "nanozyme", which is a functional term coined as early as 2007 [116]. The approach exploits the specificity of a *P. aeruginosa*-specific aptamer, termed F23.

The presence of F23 inhibits the inherent peroxidase-like activity of AuNPs by simple adsorption onto the surface of the AuNPs. However, in the presence of *P. aeruginosa*, the aptamer dissociates from the AuNP surface, thus restoring the AuNPs peroxidase-like activity for oxidation of 3,3′,5,5′-tetramethylbenzidine (TMB). As TMB is an electrochemically active species, it enables an ultrasensitive electrochemical assay using a disposable carbon screen-printed electrode. This approach allows rapid detection of *P. aeruginosa* with a LOD of ~60 CFU/mL in water within 10 min.

9.2.2. Escherichia coli

E. coli are bacteria found in the environment, foods, and intestines of people and animals. *E. coli* are a large and diverse group of bacteria. Although most strains of *E. coli* are harmless, others are not. Some kinds of *E. coli* can cause diarrhea, while others cause urinary tract infections, respiratory illness, pneumonia, and other illnesses.

The rapid and cost-effective detection of *E. coli* is of great importance to ensuring food safety by preventing food poisoning. Zhang et al. [117] developed a sensitive method for detection of *E. coli* using a

bacteria-specific aptamer in conjunction with microchip capillary electrophoresis (CE)-coupled laser-induced fluorescence. Based on the differences between charge to mass ratios of free aptamer and bacteria-aptamer complex, which influence their electrophoretic mobilities, the separation of peaks for free aptamer and bacteria-aptamer complex by microchip CE could be rapidly achieved. Under optimal conditions, detection of *E. coli* was achieved with a detection limit of 3.7 × 10² CFU/mL, at a fast response of 135 s and a short detection length of 2.3 cm. Spike-in recovery experiments showed that *E. coli* could be recovered from spiked drinking water and milk samples with recovery rates of 94.7% and 92.8%, respectively.

Zhu et al. [118] reported rapid colorimetric detection and typing of *E. coli* lipopolysaccharides (LPS) based on dual aptamer-functionalized AuNPs. Aptamers against either ethanolamine or *E. coli* O111:B4 LPS were used to separately functionalize the AuNPs. The AuNPs functionalized with the ethanolamine aptamer are termed a general probe (G-probe). The G-probe can recognize any type of LPS based on the fact that ethanolamine is a structural component of every type of LPS. This causes a sandwich-mediated aggregation of the AuNPs and a color change from red to blue. The AuNPs functionalized with the aptamer against the LPS of *E. coli* O111:B4 specifically bind to *E. coli* O111:B4 LPS and are termed the specific probe (S-probe). By using these two probes, a binary color typing method was developed. For example, G-probe and S-probe give blue and red, respectively, for *E. coli* O111:B4 LPS vs. blue and blue, respectively, for *E. coli* 055:B5 LPS.

9.2.3. Vibrio parahemolyticus

According to the CDC, *Vibrio* bacteria live in saltwater. People can get vibriosis after eating raw or undercooked shellfish, particularly oysters. Several species of *Vibrio*, including *V. parahaemolyticus*, can cause illness. Symptoms typically consist of mild to moderate diarrhea, but can sometimes be severe, especially if the bacteria enter the bloodstream. Safe shellfish preparation is necessary to avoid illness, especially among high risk people. High risk groups include people with weakened immune systems, and people with chronic liver disease.

Sun et al. [119] have reported a colorimetric aptasensor for detecting *V. parahaemolyticus* comprised of three parts: magnetic NPs (MNPs) modified with streptavidin, a biotinylated *V. parahaemolyticus* aptamer, and a label-free ssDNA that is complementary (cDNA) to the aptamer and has a G-quadruples component. The aptamer was conjugated to MNPs via the biotin−streptavidin interaction, and then the cDNA was partly hybridized with aptamer thus allowing ssDNA to attach to the surface of the MNPs. As *V. parahaemolyticus* was introduced into the assay, *V. parahaemolyticus* and cDNA compete for the binding site of the aptamer. The bacterial cells have higher binding affinity to aptamers than cDNA, thus leading to the dissociation of ssDNA from the MNPs. After magnetic pull-down of the MNPs, supernatant was collected and hemin added to form a trivalent DNAzyme by interacting with the G-quadruplex moiety. TMB (section 9.2.1.) solution containing H_2O_2 was then added to the supernatant to obtain an absorbance signal at 655 nm. By contrast, in the absence of *V. parahaemolyticus*, the supernatant did not show a significant colorimetric signal. Under optimal conditions, a wide linear detection range from 10^2 to 10^7 CFU/mL was achievable, and the detection limit was 10 CFU/mL. This method was used to detect *V. parahaemolyticus* in contaminated salmon samples, and the results showed good consistency with those obtained from a standard plate-counting method.

9.2.4. Caliciviridae (norovirus)

The *Caliciviridae* are a family of viruses that include disease-causing members such as feline calicivirus, rabbit hemorrhagic virus, and Norwalk group of viruses, among which is the well-known norovirus (NoV) that causes gastroenteritis characterized by non-bloody diarrhea, vomiting, and stomach pain. Although NoV outbreaks on cruise ships receives much attention in news media, NoV is far more widespread, resulting in about 685 million cases of disease and 200,000 deaths

globally a year.

Weerathunge et al. [120] proposed a new colorimetric nanozyme (section 9.2.1) aptasensor strategy for rapid (10 min) and ultrasensitive (calculated LOD of 200 virus particles/mL) detection of NoV based on model studies using murine norovirus (MNoV), a readily cultivable surrogate for NoV. The approach combines the enzyme-mimic catalytic activity of AuNPs with high target specificity of an MNoV aptamer to create sensor probes that produce a blue color in the presence of MNoV, in proportion to the virus concentration. Briefly, tyrosine-capped AuNPs were synthesized and the peroxidase-like nanozyme activity of the AuNPs was evaluated by measuring the oxidation of TMB substrate to a blue colored product in the presence of H_2O_2. A previously reported SELEX-selected MNoV-specific aptamer was simply adsorbed onto the surface of the AuNPs via interactions with nitrogenous nucleobases, and thus blocks nanozyme activity. The presence of MNoV leads to desorption of the aptamer and generation of color-forming nanozyme activity. The robustness of the proposed NoV nanozyme aptasensor was demonstrated by testing its performance in the presence of other nontarget microorganisms, human serum and shellfish homogenate.

In regard to the SELEX-selected MNoV-specific aptamer used by Weerathunge et al. [120] for the above-mentioned aptasensor, other investigators have recently demonstrated [121] a novel multi-well plate-based format to screen and sequence over 30 million oligonucleotides. From these, two aptamers were selected to incorporate into an RT-qPCR capture assay for successful detection of NoV in 5 clinical samples.

9.3. Pesticides

With growing environmental and health concerns over persistent organic compounds such as organophosphates, regulatory bodies have imposed strict regulations for their use and monitoring in water bodies. Although conventional analytical tools exist for the detection of organophosphorus pesticides, new strategies need to be developed to fulfil the ASSURED (affordable, sensitive, specific, user-friendly, rapid, equipment-free and deliverable to end users) criteria established by the World Health Organization. Following are three aptamer-based studies of organophosphorus pesticides aimed at fulfilling one or more of these criteria.

The nanozyme signaling methodology of Weerathunge et al. [120] mentioned in section 9.2.4. for NoV was extended to chlorpyrifos (Chl), an organophosphorus pesticide, by some of these same investigators in another report [122]. The underlying working principle of the aptasensor is based on the dynamic non-covalent interaction of a Chl-specific aptamer with the intrinsic peroxidase-mimic nanozyme activity of tyrosine-capped silver (Ag) NPs. The incorporation of the Chl-specific aptamer ensures high specificity leading to a colorimetric response specifically in the presence of Chl, while the sensor remains unresponsive to other pesticides from organophosphate and non-organophosphate groups. The functional robustness of this sensor toward environmental samples was established by evaluating its ability to detect Chl in river water samples with a 2-min sensor response time.

Jiang et al. [123] described a rapid and sensitive fluorescence assay for the detection of three organophosphorus pesticides—trichlorfon, glyphosate, and malathion—using 6-carboxy-fluorescein labeled aptamer as the probe and functionalized MNPs. Briefly, the labeled aptamer is hybridized with cDNA conjugated to the surface of the MNPs and thereby quenched. Upon introducing the target organophosphorus pesticide, the aptamer is de-hybridized from the cDNA/MNP complex, resulting in a fluorescence signal. Under optimized conditions, the LODs for trichlorfon, glyphosate, and malathion were 72.20 ng/L, 88.80 ng/L, and 195.37 ng/L, respectively. The method was applied to the detection of trichlorfon, glyphosate, and malathion in spiked lettuce and carrot samples. The recoveries were in the range of 79%–118%, which were in good agreement with those obtained by gas chromatography, and the relative standard deviations were said to be acceptable.

Xiong et al. [124] have reported an aptasensor for profenofos based on a self-assembled ssDNA aptamer and polyethylene glycol-functionalized graphene oxide (GO-PEG). The sensor employed the fluorescence "on/off" switching strategy in a single step in homogeneous solution, with PEG as a blocking agent to suppress non-specific interactions. Compared to traditional detection methods, the strategy proposed is simple, convenient, fast and sensitive. Additionally, GO-PEG shows better stability in salt solutions and is biocompatible. Profenofos was detected with an LOD of 0.21 ng/mL. This aptasensor was applied to determination of profenofos spiked into tap water, cabbage and milk with recovery values ranging from 93% to 108%, 90%–113% and 105%–114%, respectively.

10. Smartphones integrating aptamer-sensing

Decentralized analytical methods that use small portable devices for applications in the field or a doctor's office have become increasingly of interest for what are referred to as point-of-use or point-of-care, respectively. Among such devices, smartphone-based imaging, data processing, wifi, and internet technologies are attractive features to leverage in conjunction with aptamer-based detection schemes. One such example involving Cd^{2+} detection is mentioned in section 9.1.4. Many more applications based on smartphone/aptamer integration can be found in the literature; however, for the purposes of this section, three additional examples were selected from the 2019–April 2020 literature.

10.1. Cyanotoxins

Under favorable growth conditions, cyanobacteria can rapidly propagate in surface waters and produce a considerable amount of blooms (blue-green algae) along with noxious metabolites, which are designated as cyanotoxins. These toxins have caused global hazards to aquatic organisms in the marine ecosystems and posed a severe threat to human health by contaminating various water resources. Among numerous categories of cyanotoxins, microcystin-LR (MC-LR), cylindrospermopsin (CYN), nodularin (NOD), and anatoxin-a (ATX) are the most common and dangerous contaminants identified by the U.S. Environmental Protection Agency (EPA). The World Health Organization (WHO) guideline concentrations for MC-LR and CYN in drinking water are 1 μg/L, corresponding to 1–2 nM.

Li et al. [125] demonstrated a differential fluorescent sensor array made of aptamers and ssDNA-binding dyes for multiplexed detection and discrimination of these four common cyanotoxins with an ordinary smartphone within 5 min of reaction. Four aptamer sequences with high binding affinity toward the targeted cyanotoxins were selected from the literature to create a displacement fluorescent sensor array. In this assay, ssDNA-binding dyes first bind to the aptamer sequences in the absence of cyanotoxins, generating a baseline fluorescence signal. In the presence of cyanotoxins, ssDNA dyes are displaced by cyanotoxins to form a more stable cyanotoxin-aptamer complex, which results in the reduction of fluorescent intensities. The excitation wavelength and detection window were selected as close as possible to the absorption and emission peaks of the ssDNA dye to maximize the signal-to-noise ratio on the smartphone reader device (Fig. 14).

The assay reagents were preloaded and dried in a patterned microfluidic chip with a shelf-life over 60 days. Upon the addition of analyte solutions, competitive binding of cyanotoxin to the specific aptamer-dye conjugate occurred. As a result, zone-specific and concentration-dependent reduction in the green fluorescence was observed. The aptasensors were fully optimized by quantification of their dissociation constants, tuning the stoichiometric ratios of reaction mixtures, and implementation of an internal intensity correction step. The fluorescent sensor array allowed for accurate identification and measurement of ATX, CYN, NOD and MC-LR in parallel, with LODs <3 nM, close to the WHO guideline for the maximum concentration allowed in drinking
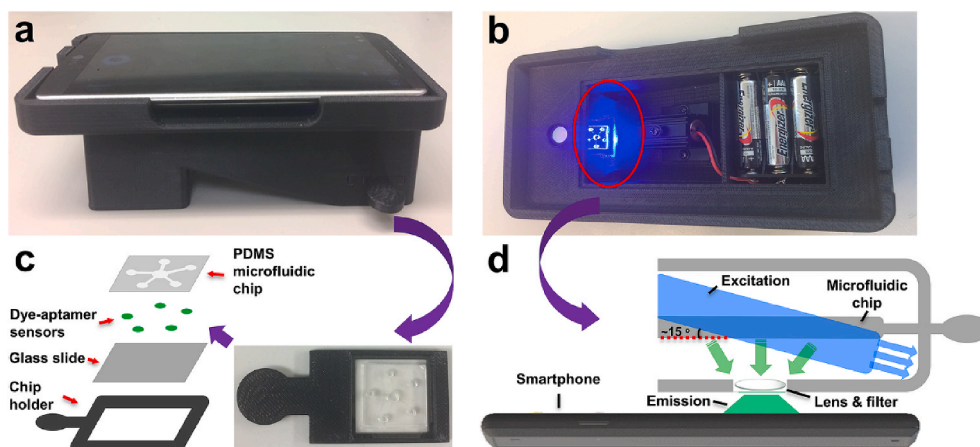
Fig. 14. Schematic illustration of the smartphone-based fluorescent detector. (a, b) Photographs of the actual smartphone reader device from different perspectives. (c) Schematic and photograph of the microfluidic chip. (d) Schematic of the optical illumination configuration. Taken from Li et al. [125] Anal. Chem. 2019, 91, 10, 448–10457 with permission. Copyright © 2019, American Chemical Society.

water. The performance of this smartphone system was tested and validated with lake water samples that were contaminated with trace levels of individual cyanotoxins as well as binary, ternary, and quaternary mixtures.

10.2. Antibiotics

Antibiotics in estuaries and groundwater generally originate from aquaculture wastewater and untreated/treated domestic sewage. These antibiotic contaminants can pose ecological and antibiotic-resistance risks, e.g. antibiotic accumulation in seafood is a risk to humans through fish consumption. Such risk has led to development of antibiotic discharge standards in aquaculture wastewater and the establishment of a standardized antibiotic monitoring and management systems.

Smartphone-based detection of two widely used antibiotics, chloramphenicol (CAP) and tetracycline (TET), was reported by Wu et al. [126], who devised a colorimetric aptasensor for multiplex antibiotics based on a ssDNA aptamer coordinately controlling aggregation of AuNPs. The multifunctional aptamer was adsorbed on AuNP surfaces acting as a binding element for CAP or TET as model antibiotics. In the presence of CAP or TET, aptamer binding occurs leading to desorption and aggregation of AuNPs to cause a change in color as the signal readout. The smartphone aptasensor exhibited selectivity and sensitivity for separate detection of TET and CAP, with LODs of 33 nM and 7 nM, respectively, and was applied to detection of these antibiotics in actual samples of interest.

10.3. Mycotoxins

A mycotoxin is a secondary metabolite produced by organisms of the fungus kingdom that is capable of causing disease and death in both humans and other animals. The term mycotoxin is usually reserved for the toxic chemical products produced by fungi that readily colonize crops, such as corn. Of these mycotoxins, aflatoxin B1 (AFB1) and ochratoxin A (OTA) are strong carcinogenic, mutagenic and cytotoxic factors. According to Ji et al. [127], traditional methods such as chromatography and mass spectrometry are accurate and sensitive, but their operation is cumbersome and requires expensive laboratory equipment and highly skilled operators. These researchers therefore developed a smartphone-based detection system for AFB1 and OTA as follows.

The scheme uses different shapes of hydrogel particles as coding elements and incorporates fluorescence image-processing techniques. In the particle preparation, two different shapes of photomasks, rectangular and circular, were used to represent the two different mycotoxins, AFB1 and OTA, as examples. AFB1- and OTA-specific aptamers are then

linked to their corresponding particle shapes. Phycoerythrin (PE)-labeled streptavidin was used to fluorescently label cDNA strands of each aptamer and thereby achieve labeling of each shaped particle. The presence of the mycotoxins leads to aptamer binding and displacement of PE-labeled cDNA that is washed away, leaving PE-labeled shaped particles for detection by PE signal imaging.

As proof-of-concept, Ji et al. [127] designed experiments to detect mycotoxins in dry corn flour by adding low, medium, and high levels (0.5, 20, and 200 ng) of mycotoxins OTA and AFB1 to dry corn flour (0.1 g). Following a simple extraction procedure (5 min) and centrifugation (10 min) the supernatant was collected, filtered and analyzed via the smartphone imaging and a standard curve. All three levels of mycotoxins were said to show satisfactory recovery (81%–121%).

11. Outlook

Extrapolation of the rate of increase in the annual number of aptamer publications indexed in PubMed indicates that there will be ~1600 articles appearing in 2025 alone, which is an average of nearly 10 publications every 2 days. Between now and then, a portion of the added aptamer-related literature will be driven by the quest for "faster, better, cheaper" performance, which are the key factors that drive innovations in biotechnology in general. Well-known examples of this include the evolution of PCR and sequencing methods, which progressed from relatively tedious and slow single-plex formats, consuming expensive reagents, to highly automated, faster methods with massive multi-plex formats affording much lower cost per sample or "answer".

While the same three "drivers" apply to aptamer-based applications, the progress has not yet been as spectacular as for PCR and sequencing over the same 30-year period starting from 1990. Nevertheless, "faster" aptamer selection protocols have been developed, as exemplified by the following two instances. In 2005, Stoltenburg et al. [128] reported use of fluorescent labels for DNA quantification and use of magnetic beads for target immobilization. Thus, radioactive labelling is avoided and immobilization on magnetic beads enables easy handling, use of very small amounts of target for the aptamer selection, rapid and efficient separation of bound and unbound molecules, and stringent washing steps. This method, termed FluMag-SELEX, has received over 350 citations in Google Scholar as of April 2020.

More recently, in 2014, Hung et al. [129] described an integrated microfluidic system capable of performing cell-SELEX for automatic, high-throughput screening of multiple cell lines to competitively select aptamer-based biomarkers exemplified in the case of ovarian cancer. This on-chip cell-SELEX process required only five rounds of aptamer selection, which is much faster than using a conventional SELEX process,

e.g. 22 rounds.

Looking forward, it is possible to envision much faster selection of aptamers leveraging the advantages provided by single-molecule nanopore sequencing [130]. For example, following a round of section from libraries of aptamers, massive numbers of bound candidate aptamers can be subjected to nanopore sequencing using the methodology recently reported by Wilson et al. [131] for handing ssDNAs with lengths in the range of typical aptamers.

With regard to "better", there have been some significant advances enabled by introduction of chemical modifications in aptamer structures, as an extension of the SOMAmer approach mentioned in section 8. In a 2017 article by Pfeiffer et al. [132] titled *Customised nucleic acid libraries for enhanced aptamer selection and performance*, it is noted that the variety of possible interactions with a putative target molecule is limited by the chemical repertoire of the natural nucleobases. Consequently, many desired targets are not addressable by aptamers. This obstacle is overcome by broadening the chemical diversity of aptamers, mainly achieved by nucleobase-modifications and the introduction of novel bases or base pairs. This chemical diversity-driver for achieving better performing aptamers has been echoed by Lokesh et al. [133] and Zon [28]. Recently, such diversity has been increased by Dunn et al. [134] using a novel xeno-nucleic acid (XNA) system in the form α-*l*-threofuranosyl nucleic acid (TNA) that is completely refractory to nuclease digestion, yet binds to HIV reverse transcriptase with Kd values of ~0.4–4.0 nM. Also, Tolle et al. [135] have extended well-known azide-alkyne cycloaddition-click chemistry [136] to the solid-phase for high fidelity synthesis of nucleobase-modified DNA aptamers dubbed "clickmers", which has the potential to greatly expand the chemical diversity of aptamers and, hence, targets for new or improved applications. XNAs and clickmers are inspiring examples of how better performance of bioanalytical applications can be derived by integrating aptamers with different technologies, namely, click chemistry and XNAs.

Another such example is evident in the integration of aptamers with powerful gene editing or interference by CRISPR (reviewed by Doudna [137] in 2020), which is challenged by the need to increase intracellular target specificity or cell delivery specificity or both in biomedical and biotechnology applications. An initial demonstration of aptamer-CRISPR integration was reported in 2017 by Zhen et al. [138], who achieved targeted delivery of CRISPR/Cas9 [137] to prostate cancer cells in vitro by modified guide RNA (gRNA) [137] using a flexible aptamer-cationic liposome for PLK-1 (section 2.) gene silencing. Later that year, Liang et al. [139] successfully extended a similar integrated approach to liposomal aptamer-targeting of CRISPR/Cas9 against vascular endothelial growth factor A in mouse models of osteosarcoma. In 2020, Xu et al. [140] reported the first example of the integration of dual aptamer technology and CRISPR-Cas12a [137]-assisted rolling circle amplification to obtain both accurate identification and highly-sensitive detection of methicillin-resistant *Staphylococcus ureus* (MRSA), detection of which is a global priority.

Finally, coronavirus disease 2019 (COVID-19), caused by the severe acute respiratory syndrome coronavirus 2 (SARS-CoV-2), which was first reported [141] in late December 2019 and quickly became a major pandemic [142], has prompted unprecedented global efforts to rapidly develop effective detection, diagnostic, therapeutic, and preventative methods to combat this crisis. The similar but less critical pandemic of SARS in 2003 led to development of aptamers for sensitive detection [143,144] of, and possible treatments [145,146] for that earlier strain of coronavirus, albeit not quickly. Advances since then leading to faster, cheaper, better aptamer technologies will hopefully enable development of important tools for COVID-19/SARS-CoV-2 much more rapidly. Indeed, in April 2020, a preprint posted by Rangan et al. [147] titled *De novo 3D models of SARS-CoV-2* RNA *elements and small-molecule-binding RNAs to guide drug discovery* is aptamer-related. Also in April 2020, Abbott et al. [148] published a paper titled *Development of CRISPR as an antiviral strategy to combat SARS-CoV-2 and influenza*. This paper

concludes that "the biggest barrier to deploying [this approach] clinically is the development of effective and safe in vivo delivery methods", and that among "several attractive delivery options that could be employed [is] DNA-based liposomal delivery strategies". Promisingly, as exemplified in this and other accounts, there are numerous examples of successful cellular targeting of liposomal delivery using aptamers to draw from.

References

[1] A.V. Lakhin, V.Z. Tarantul, L.V. Gening, Aptamers: problems, solutions and prospects, Acta Naturae 5 (2013) 34–43. https://www.ncbi.nlm.nih.gov/pubmed /24455181.

[2] S. Miersch, S.S. Sidhu, Synthetic antibodies: concepts, potential and practical considerations, Methods 57 (2012) 486–498. https://www.ncbi.nlm.nih.gov/pub med/22750306.

[3] M. Bauer, M. Strom, D.S. Hammond, S. Shigdar, Anything you can do, I can do better: can aptamers replace antibodies in clinical diagnostic applications? Molecules (2019) 24. https://www.ncbi.nlm.nih.gov/pubmed/31801185.

[4] C. Tuerk, L. Gold, Systematic evolution of ligands by exponential enrichment: RNA ligands to bacteriophage T4 DNA polymerase, Science 249 (1990) 505. http://science.sciencemag.org/content/249/4968/505.abstract.

[5] A.D. Ellington, J.W. Szostak, In vitro selection of RNA molecules that bind specific ligands, Nature 346 (1990) 818–822. https://www.ncbi.nlm.nih.gov/p ubmed/1697402.

[6] L.C. Bock, L.C. Griffin, J.A. Latham, E.H. Vermaas, J.J. Toole, Selection of single-stranded DNA molecules that bind and inhibit human thrombin, Nature 355 (1992) 564–566, https://doi.org/10.1038/355564a0.

[7] B. Thoma, T.M. Chan, Using Google Scholar to track the scholarly output of research groups, Perspect Med Educ 8 (2019) 201–205. https://www.ncbi.nlm. nih.gov/pubmed/31102192.

[8] N. Fiorini, K. Canese, R. Bryzgunov, I. Radetska, A. Gindulyte, M. Latterner, V. Miller, M. Osipov, M. Kholodov, G. Starchenko, E. Kireev, Z. Lu, PubMed Labs: an experimental system for improving biomedical literature search, Database 2018 (2018). https://www.ncbi.nlm.nih.gov/pubmed/30239682.

[9] A.B. Wagner, SciFinder Scholar 2006: an empirical analysis of research topic query processing, J. Chem. Inf. Model. 46 (2006) 767–774. https://www.ncbi. nlm.nih.gov/pubmed/16563008.

[10] N. Komarova, A. Kuznetsov, Inside the black box: what makes SELEX better? Molecules (2019) 24. https://www.ncbi.nlm.nih.gov/pubmed/31591283.

[11] F.V. Oberhaus, D. Frense, D. Beckmann, Immobilization techniques for aptamers on gold electrodes for the electrochemical detection of proteins: a review, Biosensors (2020) 10. https://www.ncbi.nlm.nih.gov/pubmed/32354207.

[12] S. Shigdar, Aptamer-based diagnostics and therapeutics, Pharmaceuticals (2019) 12. https://www.ncbi.nlm.nih.gov/pubmed/30609700.

[13] S. Zununi Vahed, N. Fathi, M. Samiei, S. Maleki Dizaj, S. Sharifi, Targeted cancer drug delivery with aptamer-functionalized polymeric nanoparticles, J. Drug Target. 27 (2019) 292–299. https://www.ncbi.nlm.nih.gov/pubmed/29929413.

[14] S.A. Moosavian, A. Sahebkar, Aptamer-functionalized liposomes for targeted cancer therapy, Canc. Lett. 448 (2019) 144–154. https://www.ncbi.nlm.nih. gov/pubmed/30763718.

[15] A. Eilers, S. Witt, J. Walter, Aptamer-modified nanoparticles in medical applications, Adv. Biochem. Eng. Biotechnol. (2020). https://www.ncbi.nlm.nih. gov/pubmed/32157319.

[16] M.W. Kim, H.Y. Jeong, S.J. Kang, I.H. Jeong, M.J. Choi, Y.M. You, C.S. Im, I. H. Song, T.S. Lee, J.S. Lee, A. Lee, Y.S. Park, Anti-EGF receptor aptamer-guided Co-delivery of anti-cancer siRNAs and quantum dots for theranostics of triple-negative breast cancer, Theranostics 9 (2019) 837–852. https://www.ncbi.nlm. nih.gov/pubmed/30809312.

[17] S. Iravani, R.S. Varma, Green synthesis, biomedical and biotechnological applications of carbon and graphene quantum dots. a review, Environ. Chem. Letts. (2020), https://doi.org/10.1007/s10311-020-00984-0.

[18] M. Caillaud, M. El Madani, L. Massad-Massade, Small interfering RNA from the lab discovery to patients' recovery, J. Contr. Release 321 (2020) 616–628. http:// www.sciencedirect.com/science/article/pii/S016836592030122X.

[19] A. Ayati, S. Moghimi, S. Salarinejad, M. Safavi, B. Pouramiri, A. Foroumadi, A review on progression of epidermal growth factor receptor (EGFR) inhibitors as an efficient approach in cancer targeted therapy, Bioorg. Chem. 99 (2020) 103811. http://www.sciencedirect.com/science/article/pii/S0045206 819319406.

[20] S. Indoria, V. Singh, M.-F. Hsieh, Recent advances in theranostic polymeric nanoparticles for cancer treatment: a review, Int. J. Pharm. 582 (2020) 119314. http://www.sciencedirect.com/science/article/pii/S0378517320302982.

[21] J. Zou, M. Shi, X. Liu, C. Jin, X. Xing, L. Qiu, W. Tan, Aptamer-functionalized exosomes: elucidating the cellular uptake mechanism and the potential for cancer-targeted chemotherapy, Anal. Chem. 91 (2019) 2425–2430. https://www.ncbi.nlm.nih.gov/pubmed/30620179.

[22] J. Daßler-Plenker, V. Küttner, M. Egeblad, Communication in tiny packages: exosomes as means of tumor-stroma communication, Biochim. Biophys. Acta Rev. Canc 1873 (2020) 188340. http://www.sciencedirect.com/science/article/pii/S0304419X1930201X.

[23] D. Shangguan, Y. Li, Z. Tang, Z.C. Cao, H.W. Chen, P. Mallikaratchy, K. Sefah, C. J. Yang, W. Tan, Aptamers evolved from live cells as effective molecular probes for cancer study, Proc. Natl. Acad. Sci. USA. 103 (2006) 11838. http://www.pnas.org/content/103/32/11838.abstract.

[24] W. Zhong, Y. Pu, W. Tan, J. Liu, J. Liao, B. Liu, K. Chen, B. Yu, Y. Hu, Y. Deng, J. Zhang, H. Liu, Identification and application of an aptamer targeting papillary thyroid carcinoma using tissue-SELEX, Anal. Chem. 91 (2019) 8289–8297. https://www.ncbi.nlm.nih.gov/pubmed/31141341.

[25] V. Domenyuk, Z. Gatalica, R. Santhanam, X. Wei, A. Stark, P. Kennedy, B. Toussaint, S. Levenberg, J. Wang, N. Xiao, R. Greil, G. Rinnerthaler, S. P. Gampenrieder, A.B. Heimberger, D.A. Berry, A. Barker, J. Quackenbush, J. L. Marshall, G. Poste, J.L. Vacirca, G.A. Vidal, L.S. Schwartzberg, D.D. Halbert, A. Voss, D. Magee, M.R. Miglarese, M. Famulok, G. Mayer, D. Spetzler, Poly-ligand profiling differentiates trastuzumab-treated breast cancer patients according to their outcomes, Nat. Commun. 9 (2018) 1219, https://doi.org/10.1038/s41467-018-03631-z.

[26] R. Yazdian-Robati, P. Bayat, F. Oroojalian, M. Zargari, M. Ramezani, S. M. Taghdisi, K. Abnous, Therapeutic applications of AS1411 aptamer, an update review, Int. J. Biol. Macromol. (2019). http://www.sciencedirect.com/science/article/pii/S0141813019374756.

[27] X. Fan, L. Sun, Y. Wu, L. Zhang, Z. Yang, Bioactivity of 2′-deoxyinosine-incorporated aptamer AS1411, Sci. Rep. 6 (2016) 25799, https://doi.org/10.1038/srep25799.

[28] G. Zon, CHAPTER 16 Aptamers and Clinical Applications, Advances in Nucleic Acid Therapeutics, The Royal Society of Chemistry, 2019, pp. 367–399, https://doi.org/10.1039/9781788015714-00367.

[29] M. Klanova, P. Klener, BCL-2 proteins in pathogenesis and therapy of B-cell non-hodgkin lymphomas, Cancers (2020) 12. https://www.ncbi.nlm.nih.gov/pubmed/32290241.

[30] S. Yu, X. Bi, L. Yang, S. Wu, Y. Yu, B. Jiang, A. Zhang, K. Lan, S. Duan, Co-delivery of paclitaxel and PLK1-targeted siRNA using aptamer-functionalized cationic liposome for synergistic anti-breast cancer effects in vivo, J. Biomed. Nanotechnol. 15 (2019) 1135–1148. https://www.ncbi.nlm.nih.gov/pubmed/31072423.

[31] S. Kumar, J. Kim, PLK-1 targeted inhibitors and their potential against tumorigenesis, BioMed Res. Int. 2015 (2015) 705745. https://www.ncbi.nlm.nih.gov/pubmed/26557691.

[32] T. Kong, R. Zhou, Y. Zhang, L. Hao, X. Cai, B. Zhu, AS1411 aptamer modified carbon dots via polyethylenimine-assisted strategy for efficient targeted cancer cell imaging, Cell Prolif 53 (2020), e12713. https://www.ncbi.nlm.nih.gov/pubmed/31691382.

[33] L. Alizadeh, E. Alizadeh, A. Zarebkohan, E. Ahmadi, M. Rahmati-Yamchi, R. Salehi, AS1411 aptamer-functionalized chitosan-silica nanoparticles for targeted delivery of epigallocatechin gallate to the SKOV-3 ovarian cancer cell lines, J. Nanoparticle Res. 22 (2020) 5, https://doi.org/10.1007/s11051-019-4735-7.

[34] D. Wu, L. Zhu, Y. Li, X. Zhang, S. Xu, G. Yang, T. Delair, Chitosan-based colloidal polyelectrolyte complexes for drug delivery: a review, Carbohydr. Polym. 238 (2020) 116126. http://www.sciencedirect.com/science/article/pii/S0144861720303003.

[35] R. Moody, K. Wilson, A. Jaworowski, M. Plebanski, Natural Compounds with Potential to Modulate Cancer Therapies and Self-Reactive Immune Cells, Cancers (Basel), 2020, p. 12. https://www.ncbi.nlm.nih.gov/pubmed/32183059.

[36] N. Hamaguchi, A. Ellington, M. Stanton, Aptamer beacons for the direct detection of proteins, Anal. Biochem. 294 (2001) 126–131. https://www.ncbi.nlm.nih.gov/pubmed/11444807.

[37] X. Fang, J.J. Li, J. Perlette, W. Tan, K. Wang, Molecular beacons: novel fluorescent probes, Anal. Chem. 72 (2000) 747A–753A. https://www.ncbi.nlm.nih.gov/pubmed/11128959.

[38] A. Moutsiopoulou, D. Broyles, E. Dikici, S. Daunert, S.K. Deo, Molecular aptamer beacons and their applications in sensing, imaging, and diagnostics, Small 15 (2019), e1902248. https://www.ncbi.nlm.nih.gov/pubmed/31313884.

[39] Y. Peng, D. Li, R. Yuan, Y. Xiang, A catalytic and dual recycling amplification ATP sensor based on target-driven allosteric structure switching of aptamer beacons, Biosens. Bioelectron. 105 (2018) 1–5. https://www.ncbi.nlm.nih.gov/pubmed/29331900.

[40] J. Liu, Y. Zhang, H. Xie, L. Zhao, L. Zheng, H. Ye, Applications of catalytic hairpin assembly reaction in biosensing, Small 15 (2019) 1902989. https://onlinelibrary.wiley.com/doi/abs/10.1002/smll.201902989.

[41] L. Xu, B. Jiang, W. Zhou, R. Yuan, Y. Xiang, Coupling strand extension/excision amplification with target recycling enables highly sensitive and aptamer-based label-free sensing of ATP in human serum, Analyst 145 (2020) 434–439. https://www.ncbi.nlm.nih.gov/pubmed/31793560.

[42] X.-N. Feng, Y.-X. Cui, J. Zhang, A.-N. Tang, H.-B. Mao, D.-M. Kong, Chiral interaction is a decisive factor to replace d-DNA with l-DNA aptamers, Anal. Chem. (2020), https://doi.org/10.1021/acs.analchem.9b05676.

[43] S. Yoon, J.J. Rossi, Targeted molecular imaging using aptamers in cancer, Pharmaceuticals (2018) 11. https://www.ncbi.nlm.nih.gov/pubmed/30029472.

[44] S. Nath, P. Mukherjee, MUC1: a multifaceted oncoprotein with a key role in cancer progression, Trends Mol. Med. 20 (2014) 332–342. https://www.ncbi.nlm.nih.gov/pubmed/24667139.

[45] Q. Zou, C.-J. Zhang, Y.-Z. Yan, Z.-J. Min, C.-S. Li, MUC-1 aptamer targeted superparamagnetic iron oxide nanoparticles for magnetic resonance imaging of pancreatic cancer in vivo and in vitro experiment, J. Cell. Biochem. 120 (2019) 18650–18658, https://doi.org/10.1002/jcb.28950.

[46] Y. Wang, X. Li, P. Chen, Y. Dong, G. Liang, Y. Yu, Enzyme-instructed self-aggregation of Fe3O4 nanoparticles for enhanced MRI T2 imaging and photothermal therapy of tumors, Nanoscale 12 (2020) 1886–1893, https://doi.org/10.1039/C9NR09235H.

[47] M. Trzpis, P.M.J. McLaughlin, L.M.F.H. de Leij, M.C. Harmsen, Epithelial cell adhesion molecule: more than a carcinoma marker and adhesion molecule, Am. J. Pathol. 171 (2007) 386–395, https://doi.org/10.2353/ajpath.2007.070152.

[48] X. Guo, X. Wu, M. Sun, L. Xu, H. Kuang, C. Xu, Tetrahedron probes for ultrasensitive in situ detection of telomerase and surface glycoprotein activity in living cells, Anal. Chem. 92 (2020) 2310–2315, https://doi.org/10.1021/acs.analchem.9b05180.

[49] N. Xie, H. Wang, K. Quan, F. Feng, J. Huang, K. Wang, Self-assembled DNA-Based geometric polyhedrons: construction and applications, Trac. Trends Anal. Chem. 126 (2020) 115844. http://www.sciencedirect.com/science/article/pii/S0165993619306843.

[50] G.S. Zamay, O.S. Kolovskaya, T.I. Ivanchenko, T.N. Zamay, D.V. Veprintsev, V. L. Grigorieva, Garanzha II, A.V. Krat, Y.E. Glazyrin, A. Gargaun, I.N. Lapin, V. A. Svetlichnyi, M.V. Berezovski, A.S. Kichkailo, Development of DNA aptamers to native EpCAM for isolation of lung circulating tumor cells from human blood, Cancers (2019) 11. https://www.ncbi.nlm.nih.gov/pubmed/30871104.

[51] D.R. Bell, J.K. Weber, W. Yin, T. Huynh, W. Duan, R. Zhou, In silico design and validation of high-affinity RNA aptamers targeting epithelial cellular adhesion molecule dimers, Proc. Natl. Acad. Sci. USA. 117 (2020) 8486. http://www.pnas.org/content/117/15/8486.abstract.

[52] S. Shigdar, C. Qian, L. Lv, C. Pu, Y. Li, L. Li, M. Marappan, J. Lin, L. Wang, W. Duan, The use of sensitive chemical antibodies for diagnosis: detection of low levels of EpCAM in breast cancer, PloS One 8 (2013), e57613. https://www.ncbi.nlm.nih.gov/pubmed/23460885.

[53] L. Shen, T. Bing, N. Zhang, L. Wang, J. Wang, X. Liu, D. Shangguan, A nucleus-targeting DNA aptamer for dead cell indication, ACS Sens. 4 (2019) 1612–1618. https://www.ncbi.nlm.nih.gov/pubmed/31099246.

[54] T. Ramamurthy, A. Ghosh, G.P. Pazhani, S. Shinoda, Current perspectives on viable but non-culturable (VBNC) pathogenic bacteria, Front. Pub. Health 2 (2014). https://www.frontiersin.org/article/10.3389/fpubh.2014.00103.

[55] D. Liu, B. Hu, D. Peng, S. Lu, S. Gao, Z. Li, L. Wang, B. Jiao, Isolation ssDNA aptamers specific for both live and viable but nonculturable state Vibrio vulnificus using whole bacteria-SEILEX technology, RSC Adv. 10 (2020) 15997–16008, https://doi.org/10.1039/C9RA10733A.

[56] J.S. Paige, K.Y. Wu, S.R. Jaffrey, RNA mimics of green fluorescent protein, Science 333 (2011) 642–646. https://www.ncbi.nlm.nih.gov/pubmed/21798953.

[57] R. Wirth, P. Gao, G.U. Nienhaus, M. Sunbul, A. Jaschke, SiRA: a silicon rhodamine-binding aptamer for live-cell super-resolution RNA imaging, J. Am. Chem. Soc. 141 (2019) 7562–7571. https://www.ncbi.nlm.nih.gov/pubmed/30986047.

[58] C.G. Galbraith, J.A. Galbraith, Super-resolution microscopy at a glance, J. Cell Sci. 124 (2011) 1607. http://jcs.biologists.org/content/124/10/1607.abstract.

[59] J. Wu, S. Zaccara, D. Khuperkar, H. Kim, M.E. Tanenbaum, S.R. Jaffrey, Live imaging of mRNA using RNA-stabilized fluorogenic proteins, Nat. Methods 16 (2019) 862–865, https://doi.org/10.1038/s41592-019-0531-7.

[60] K.M. Bonger, L.C. Chen, C.W. Liu, T.J. Wandless, Small-molecule displacement of a cryptic degron causes conditional protein degradation, Nat. Chem. Biol. 7 (2011) 531–537. https://www.ncbi.nlm.nih.gov/pubmed/21725303.

[61] D.P. Bartel, MicroRNAs: target recognition and regulatory functions, Cell 136 (2009) 215–233. https://www.ncbi.nlm.nih.gov/pubmed/19167326.

[62] J.S. Hartig, I. Grune, S.H. Najafi-Shoushtari, M. Famulok, Sequence-specific detection of MicroRNAs by signal-amplifying ribozymes, J. Am. Chem. Soc. 126 (2004) 722–723. https://www.ncbi.nlm.nih.gov/pubmed/14733539.

[63] W. Zhong, J.T. Sczepanski, A mirror image fluorogenic aptamer sensor for live-cell imaging of MicroRNAs, ACS Sens. 4 (2019) 566–570. https://www.ncbi.nlm.nih.gov/pubmed/30843691.

[64] B.E. Young, N. Kundu, J.T. Sczepanski, Mirror-image oligonucleotides: history and emerging applications, Chem. Eur J. 25 (2019) 7981–7990. https://chemistry-europe.onlinelibrary.wiley.com/doi/abs/10.1002/chem.201900149.

[65] A. Autour, S.C.Y. Jeng, A.D. Cawte, A. Abdolahzadeh, A. Galli, S.S. Panchapakesan, D. Rueda, M. Ryckelynck, P.J. Unrau, Fluorogenic RNA Mango aptamers for imaging small non-coding RNAs in mammalian cells, Nat. Commun. 9 (2018) 656, https://doi.org/10.1038/s41467-018-02993-8.

[66] Y. Xu, J.A. Phillips, J. Yan, Q. Li, Z.H. Fan, W. Tan, Aptamer-based microfluidic device for enrichment, sorting, and detection of multiple cancer cells, Anal. Chem. 81 (2009) 7436–7442, https://doi.org/10.1021/ac9012072.

[67] U. Dharmasiri, S. Balamurugan, A.A. Adams, P.I. Okagbare, A. Obubuafo, S. A. Soper, Highly efficient capture and enumeration of low abundance prostate cancer cells using prostate-specific membrane antigen aptamers immobilized to a

polymeric microfluidic device, Electrophoresis 30 (2009) 3289–3300. https ://www.ncbi.nlm.nih.gov/pubmed/19722212.

[68] C. Alix-Panabières, K. Pantel, Clinical applications of circulating tumor cells and circulating tumor DNA as liquid biopsy, Canc. Discov. 6 (2016) 479. http://cance rdiscovery.aacrjournals.org/content/6/5/479.abstract.

[69] J. Kaiser, Cancer DNA blood test gets real-world trial, Science 368 (2020) 461. http://science.sciencemag.org/content/368/6490/461.abstract.

[70] M.W. Snyder, M. Kircher, A.J. Hill, R.M. Daza, J. Shendure, Cell-free DNA comprises an in vivo nucleosome footprint that informs its tissues-of-origin, Cell 164 (2016) 57–68. https://www.ncbi.nlm.nih.gov/pubmed/26771485.

[71] N. Ogawa, M.D. Biggin, High-throughput SELEX determination of DNA sequences bound by transcription factors in vitro, Methods Mol. Biol. 786 (2012) 51–63. https://www.ncbi.nlm.nih.gov/pubmed/21938619.

[72] L. Wu, L. Zhu, M. Huang, J. Song, H. Zhang, Y. Song, W. Wang, C. Yang, Aptamer-based microfluidics for isolation, release and analysis of circulating tumor cells, Trac. Trends Anal. Chem. 117 (2019) 69–77. http://www.sciencedirect.com/sci ence/article/pii/S0165993619301669.

[73] Y. Song, Y. Shi, M. Huang, W. Wang, Y. Wang, J. Cheng, Z. Lei, Z. Zhu, C. Yang, Bioinspired engineering of a multivalent aptamer-functionalized nanointerface to enhance the capture and release of circulating tumor cells, Angew Chem. Int. Ed. Engl. 58 (2019) 2236–2240. https://www.ncbi.nlm.nih.gov/pubmed/30548959.

[74] Z. Liu, F. Huang, J. Du, W. Shu, H. Feng, X. Xu, Y. Chen, Rapid isolation of cancer cells using microfluidic deterministic lateral displacement structure, Biomicrofluidics 7 (2013), 011801, https://doi.org/10.1063/1.4774308.

[75] Y. Song, Z. Zhu, Y. An, W. Zhang, H. Zhang, D. Liu, C. Yu, W. Duan, C.J. Yang, Selection of DNA aptamers against epithelial cell adhesion molecule for cancer cell imaging and circulating tumor cell capture, Anal. Chem. 85 (2013) 4141–4149, https://doi.org/10.1021/ac400366b.

[76] J. Yang, X. Li, B. Jiang, R. Yuan, Y. Xiang, In situ-generated multivalent aptamer network for efficient capture and sensitive electrochemical detection of circulating tumor cells in whole blood, Anal. Chem. (2020), https://doi.org/10.1021/acs.analchem.0c01195.

[77] D. Ou, D. Sun, Z. Liang, B. Chen, X. Lin, Z. Chen, A novel cytosensor for capture, detection and release of breast cancer cells based on metal organic framework PCN-224 and DNA tetrahedron linked dual-aptamer, Sensor. Actuator. B Chem. 285 (2019) 398–404. http://www.sciencedirect.com/science/article/pii/S0 92540051930108X.

[78] L. Du, W. Chen, P. Zhu, Y. Tian, Y. Chen, C. Wu, Applications of functional metal-organic frameworks in biosensors, Biotechnol. J. (2020) 1900424, https://doi.org/10.1002/biot.201900424, n/a.

[79] T. Yan, L. Zhu, H. Ju, J. Lei, DNA-Walker-Induced allosteric switch for tandem signal amplification with palladium nanoparticles/metal–organic framework tags in electrochemical biosensing, Anal. Chem. 90 (2018) 14493–14499, https://doi.org/10.1021/acs.analchem.8b04338.

[80] X.-H. Zhou, D.-M. Kong, H.-X. Shen, G-quadruplex–hemin DNAzyme-amplified colorimetric detection of Ag+ ion, Anal. Chim. Acta 678 (2010) 124–127. http://www.sciencedirect.com/science/article/pii/S0003267010010536.

[81] A. Tahiri-Alaoui, L. Frigotto, N. Manville, J. Ibrahim, P. Romby, W. James, High affinity nucleic acid aptamers for streptavidin incorporated into bi-specific capture ligands, Nucleic Acids Res. 30 (2002) e45. https://www.ncbi.nlm.nih.gov/pubmed/12000850.

[82] C. Persson, E.G. Wagner, K. Nordström, Control of replication of plasmid R1: structures and sequences of the antisense RNA, CopA, required for its binding to the target RNA, CopT, EMBO J. 9 (1990) 3767–3775. https://pubmed.ncbi.nlm.nih.gov/1698621. https://www.ncbi.nlm.nih.gov/pmc/articles/PMC552134/.

[83] F. Pastor, D. Kolonias, J.O. McNamara 2nd, E. Gilboa, Targeting 4-1BB costimulation to disseminated tumor lesions with bi-specific oligonucleotide aptamers, Mol. Ther. 19 (2011) 1878–1886. https://www.ncbi.nlm.nih.gov/pub med/21829171.

[84] A. Boltz, B. Piater, L. Toleikis, R. Guenther, H. Kolmar, B. Hock, Bi-specific aptamers mediating tumor cell lysis, J. Biol. Chem. 286 (2011) 21896–21905. https://www.ncbi.nlm.nih.gov/pubmed/21531729.

[85] X. Liu, H. Yan, Y. Liu, Y. Chang, Targeted cell-cell interactions by DNA nanoscaffold-templated multivalent bispecific aptamers, Small 7 (2011) 1673–1682. https://www.ncbi.nlm.nih.gov/pubmed/21538862.

[86] M. Passariello, S. Camorani, C. Vetrei, L. Cerchia, C. De Lorenzo, Novel human bispecific aptamer-antibody conjugates for efficient cancer cell killing, Cancers (2019) 11. https://www.ncbi.nlm.nih.gov/pubmed/31470510.

[87] J. Jung, A.W. Lifland, C. Zurla, E.J. Alonas, P.J. Santangelo, Quantifying RNA–protein interactions in situ using modified-MTRIPs and proximity ligation, Nucleic Acids Res. 41 (2012), https://doi.org/10.1093/nar/gks837 e12-e12.

[88] Z. Li, Y. Hu, Y. An, J. Duan, X. Li, X.D. Yang, Novel bispecific aptamer enhances immune cytotoxicity against MUC1-positive tumor cells by MUC1-CD16 dual targeting, Molecules (2019) 24. https://www.ncbi.nlm.nih.gov/pubmed /30699986.

[89] H. Shi, Y. Lei, J. Ge, X. He, W. Cui, X. Ye, J. Liu, K. Wang, A simple, pH-activatable fluorescent aptamer probe with ultralow background for bispecific tumor imaging, Anal. Chem. 91 (2019) 9154–9160. https://www.ncbi.nlm.nih.gov/pubmed/31185714.

[90] Y. Lei, X. He, J. Tang, H. Shi, D. He, L. Yan, J. Liu, Y. Zeng, K. Wang, Ultra-pH-responsive split i-motif based aptamer anchoring strategy for specific activatable imaging of acidic tumor microenvironment, Chem Commun 54 (2018) 10288–10291. https://www.ncbi.nlm.nih.gov/pubmed/30137061.

[91] R. Liu, Y. Zhang, X. Zhao, A. Agarwal, L.J. Mueller, P. Feng, pH-responsive nanogated ensemble based on gold-capped mesoporous silica through an acid-labile acetal linker, J. Am. Chem. Soc. 132 (2010) 1500–1501, https://doi.org/10.1021/ja907838s.

[92] J.C. Rohloff, A.D. Gelinas, T.C. Jarvis, U.A. Ochsner, D.J. Schneider, L. Gold, N. Janjic, Nucleic acid ligands with protein-like side chains: modified aptamers and their use as diagnostic and therapeutic agents, Mol. Ther. Nucleic Acids 3 (2014), e201. https://www.ncbi.nlm.nih.gov/pubmed/25291143.

[93] F. Pfeiffer, M. Rosenthal, J. Siegl, J. Ewers, G. Mayer, Customised nucleic acid libraries for enhanced aptamer selection and performance, Curr. Opin. Biotechnol. 48 (2017) 111–118. http://www.sciencedirect.com/science/article/pii/S0958166917300502.

[94] J.D. McFadyen, J. Zeller, L.A. Potempa, G.A. Pietersz, S.U. Eisenhardt, K. Peter, C-reactive protein and its structural isoforms: an evolutionary conserved marker and central player in inflammatory diseases and beyond, Subcell. Biochem. 94 (2020) 499–520. https://www.ncbi.nlm.nih.gov/pubmed/32189313.

[95] M. António, R. Ferreira, R. Vitorino, A.L. Daniel-da-Silva, A simple aptamer-based colorimetric assay for rapid detection of C-reactive protein using gold nanoparticles, Talanta 214 (2020) 120868. http://www.sciencedirect.com/scienc e/article/pii/S0039914020301594.

[96] H. Minagawa, Y. Kataoka, H. Fujita, M. Kuwahara, K. Horii, I. Shiratori, I. Waga, Modified DNA aptamers for C-reactive protein and lactate dehydrogenase-5 with sub-nanomolar affinities, Int. J. Mol. Sci. 21 (2020). https://www.ncbi.nlm.nih.gov/pubmed/32294882.

[97] J. Berriman, L.C. Serpell, K.A. Oberg, A.L. Fink, M. Goedert, R.A. Crowther, Tau filaments from human brain and from in vitro assembly of recombinant protein show cross-β structure, in: Proceedings of the National Academy of Sciences, 100, 2003, p. 9034. http://www.pnas.org/content/100/1 5/9034.abstract.

[98] I.T. Teng, X. Li, H.A. Yadikar, Z. Yang, L. Li, Y. Lyu, X. Pan, K.K. Wang, W. Tan, Identification and characterization of DNA aptamers specific for phosphorylation epitopes of tau protein, J. Am. Chem. Soc. 140 (2018) 14314–14323, https://doi.org/10.1021/jacs.8b08645.

[99] I. Ziu, E.T. Laryea, F. Alashkar, C.G. Wu, S. Martic, A dip-and-read optical aptasensor for detection of tau protein, Anal. Bioanal. Chem. 412 (2020) 1193–1201, https://doi.org/10.1007/s00216-019-02350-8.

[100] A. Mechaly, H. Cohen, O. Cohen, O. Mazor, A biolayer interferometry-based assay for rapid and highly sensitive detection of biowarfare agents, Anal. Biochem. 506 (2016) 22–27. http://www.sciencedirect.com/science/article/pii/S0003269 716300604.

[101] A. Perrier, J. Gligorov, G. Lefèvre, M. Boissan, The extracellular domain of Her2 in serum as a biomarker of breast cancer, Lab. Invest. 98 (2018) 696–707, https://doi.org/10.1038/s41374-018-0033-8.

[102] D. Sanchez-Calderon, A. Pedraza, C. Mancera Urrego, A. Mejia-Mejia, A. L. Montealegre-Paez, S. Perdomo, Analysis of the cost-effectiveness of liquid biopsy to determine treatment change in patients with her2-positive advanced breast cancer in Colombia, Clinicoecon Outcomes Res 12 (2020) 115–122. https ://www.ncbi.nlm.nih.gov/pubmed/32104023.

[103] V. Ranganathan, S. Srinivasan, A. Singh, M.C. DeRosa, An aptamer-based colorimetric lateral flow assay for the detection of human epidermal growth factor receptor 2 (HER2), Anal. Biochem. 588 (2020) 113471. http://www.scienc edirect.com/science/article/pii/S0003269719307663.

[104] F. Li, Z. Yu, X. Han, R.Y. Lai, Electrochemical aptamer-based sensors for food and water analysis: a review, Anal. Chim. Acta 1051 (2019) 1–23. https://www.ncbi.nlm.nih.gov/pubmed/30661605.

[105] S.C.G. Kiruba Daniel, A. Kumar, K. Sivasakthi, C.S. Thakur, Handheld, low-cost electronic device for rapid, real-time fluorescence-based detection of Hg2+, using aptamer-templated ZnO quantum dots, Sensor. Actuator. B Chem. 290 (2019) 73–78. http://www.sciencedirect.com/science/article/pii/S0925400519304800.

[106] H. Guo, J. Li, Y. Li, D. Wu, H. Ma, Q. Wei, B. Du, Exciton energy transfer-based fluorescent sensor for the detection of Hg(2+) through aptamer-programmed self-assembly of QDs, Anal. Chim. Acta 1048 (2019) 161–167. https://www.ncbi.nlm.nih.gov/pubmed/30598146.

[107] X. Si, S. Tang, K. Wang, G. Zhou, J. Xia, Y. Zhao, H. Zhao, Q. Shen, Z. Liu, Electrochemical amplification for Hg(II) quantification by anchoring an enzymatically extended aptamer, Anal. Lett. 52 (2019) 2883–2895, https://doi.org/10.1080/00032719.2019.1626415.

[108] H. Abu-Ali, A. Nabok, T.J. Smith, Development of novel and highly specific ssDNA-aptamer-based electrochemical biosensor for rapid detection of mercury (II) and lead (II) ions in water, Chemosensors 7 (2019) 27. https://www.mdpi.com/2227-9040/7/2/27.

[109] A.N. Berlina, A.V. Zherdev, S.M. Pridvorova, M.S. Gaur, B.B. Dzantiev, Rapid visual detection of lead and mercury via enhanced crosslinking aggregation of aptamer-labeled gold nanoparticles, J. Nanosci. Nanotechnol. 19 (2019) 5489–5495. https://www.ncbi.nlm.nih.gov/pubmed/30961701.

[110] S.H. Yu, C.S. Lee, T.H. Kim, Electrochemical detection of ultratrace lead ion through attaching and detaching DNA aptamer from electrochemically reduced graphene oxide electrode, Nanomaterials (2019) 9. https://www.ncbi.nlm.nih.gov/pubmed/31151250.

[111] M. Kim, H.J. Um, S. Bang, S.H. Lee, S.J. Oh, J.H. Han, K.W. Kim, J. Min, Y.H. Kim, Arsenic removal from Vietnamese groundwater using the arsenic-binding DNA aptamer, Environ. Sci. Technol. 43 (2009) 9335–9340. https://www.ncbi.nlm.nih.gov/pubmed/20000526.

[112] K. Matsunaga, Y. Okuyama, R. Hirano, S. Okabe, M. Takahashi, H. Satoh, Development of a simple analytical method to determine arsenite using a DNA aptamer and gold nanoparticles, Chemosphere 224 (2019) 538–543. https ://www.ncbi.nlm.nih.gov/pubmed/30836249.

[113] R. Yadav, V. Kushwah, M.S. Gaur, S. Bhadauria, A.N. Berlina, A.V. Zherdev, B. B. Dzantiev, Electrochemical aptamer biosensor for As3+ based on apta deep trapped Ag-Au alloy nanoparticles-impregnated glassy carbon electrode, Int. J. Environ. Anal. Chem. 100 (2020) 623–634, https://doi.org/10.1080/03067319.2019.1638371.

[114] L. Xu, J. Liang, Y. Wang, S. Ren, J. Wu, H. Zhou, Z. Gao, Highly selective, aptamer-based, ultrasensitive nanogold colorimetric smartphone readout for detection of Cd(II), Molecules (2019) 24. https://www.ncbi.nlm.nih.gov/pubmed/31362377.

[115] R. Das, A. Dhiman, A. Kapil, V. Bansal, T.K. Sharma, Aptamer-mediated colorimetric and electrochemical detection of Pseudomonas aeruginosa utilizing peroxidase-mimic activity of gold NanoZyme, Anal. Bioanal. Chem. 411 (2019) 1229–1238. https://www.ncbi.nlm.nih.gov/pubmed/30637436.

[116] E.V. Batrakova, S. Li, A.D. Reynolds, R.L. Mosley, T.K. Bronich, A.V. Kabanov, H. E. Gendelman, A Macrophage−Nanozyme delivery system for Parkinson's disease, Bioconjugate Chem. 18 (2007) 1498–1506, https://doi.org/10.1021/bc700184b.

[117] Y. Zhang, L. Zhu, P. He, F. Zi, X. Hu, Q. Wang, Sensitive assay of Escherichia coli in food samples by microchip capillary electrophoresis based on specific aptamer binding strategy, Talanta 197 (2019) 284–290. https://www.ncbi.nlm.nih.gov/pubmed/30771937.

[118] L. Zhu, S. Li, X. Shao, Y. Feng, P. Xie, Y. Luo, K. Huang, W. Xu, Colorimetric detection and typing of E. coli lipopolysaccharides based on a dual aptamer-functionalized gold nanoparticle probe, Mikrochim. Acta 186 (2019) 111. https://www.ncbi.nlm.nih.gov/pubmed/30637507.

[119] Y. Sun, N. Duan, P. Ma, Y. Liang, X. Zhu, Z. Wang, Colorimetric aptasensor based on truncated aptamer and trivalent DNAzyme for Vibrio parahemolyticus determination, J. Agric. Food Chem. 67 (2019) 2313–2320. https://www.ncbi.nlm.nih.gov/pubmed/30721047.

[120] P. Weerathunge, R. Ramanathan, V.A. Torok, K. Hodgson, Y. Xu, R. Goodacre, B. K. Behera, V. Bansal, Ultrasensitive colorimetric detection of murine norovirus using NanoZyme aptasensor, Anal. Chem. 91 (2019) 3270–3276, https://doi.org/10.1021/acs.analchem.8b03300.

[121] D. Liu, Z. Zhang, Y. Yin, F. Jia, Q. Wu, P. Tian, D. Wang, Development and evaluation of a novel in situ target-capture approach for aptamer selection of human noroviruses, Talanta 193 (2019) 199–205. http://www.sciencedirect.com/science/article/pii/S0039914018310026.

[122] P. Weerathunge, B.K. Behera, S. Zihara, M. Singh, S.N. Prasad, S. Hashmi, P.R. D. Mariathomas, V. Bansal, R. Ramanathan, Dynamic interactions between peroxidase-mimic silver NanoZymes and chlorpyrifos-specific aptamers enable highly-specific pesticide sensing in river water, Anal. Chim. Acta 1083 (2019) 157–165. http://www.sciencedirect.com/science/article/pii/S0003267019309043.

[123] M. Jiang, C. Chen, J. He, H. Zhang, Z. Xu, Fluorescence assay for three organophosphorus pesticides in agricultural products based on Magnetic-Assisted fluorescence labeling aptamer probe, Food Chem. 307 (2020) 125534. http://www.sciencedirect.com/science/article/pii/S030881461931653X.

[124] J.e. Xiong, S. Li, Y. Li, Y. Chen, Y. Liu, J. Gan, J. Ju, Y. Xian, X. Xiong, Fluorescent aptamer-polyethylene glycol functionalized graphene oxide biosensor for profenofos detection in food, Chem. Res. Chin. Univ. (2019), https://doi.org/10.1007/s40242-019-9257-4.

[125] Z. Li, S. Zhang, T. Yu, Z. Dai, Q. Wei, Aptamer-based fluorescent sensor array for multiplexed detection of cyanotoxins on a smartphone, Anal. Chem. 91 (2019) 10448–10457. https://www.ncbi.nlm.nih.gov/pubmed/31192585.

[126] Y.Y. Wu, P. Huang, F.Y. Wu, A label-free colorimetric aptasensor based on controllable aggregation of AuNPs for the detection of multiplex antibiotics, Food Chem. 304 (2020) 125377. https://www.ncbi.nlm.nih.gov/pubmed/31476547.

[127] W. Ji, Z. Zhang, Y. Tian, Z. Yang, Z. Cao, L. Zhang, Y. Qi, J. Chang, S. Zhang, H. Wang, Shape coding microhydrogel for a real-time mycotoxin detection system based on smartphones, ACS Appl. Mater. Interfaces 11 (2019) 8584–8590. https://www.ncbi.nlm.nih.gov/pubmed/30715838.

[128] R. Stoltenburg, C. Reinemann, B. Strehlitz, FluMag-SELEX as an advantageous method for DNA aptamer selection, Anal. Bioanal. Chem. 383 (2005) 83–91. https://www.ncbi.nlm.nih.gov/pubmed/16052344.

[129] L.Y. Hung, C.H. Wang, K.F. Hsu, C.Y. Chou, G.B. Lee, An on-chip Cell-SELEX process for automatic selection of high-affinity aptamers specific to different histologically classified ovarian cancer cells, Lab Chip 14 (2014) 4017–4028. https://www.ncbi.nlm.nih.gov/pubmed/25144781.

[130] C.F. Minervini, C. Cumbo, P. Orsini, L. Anelli, A. Zagaria, G. Specchia, F. Albano, Nanopore sequencing in blood diseases: a wide range of opportunities, Front. Genet. 11 (2020). https://www.frontiersin.org/article/10.3389/fgene.2020.00076.

[131] B.D. Wilson, M. Eisenstein, H.T. Soh, High-fidelity nanopore sequencing of ultra-short DNA targets, Anal. Chem. 91 (2019) 6783–6789, https://doi.org/10.1021/acs.analchem.9b00856.

[132] F. Pfeiffer, M. Rosenthal, J. Siegl, J. Ewers, G. Mayer, Customised nucleic acid libraries for enhanced aptamer selection and performance, Curr. Opin. Biotechnol. 48 (2017) 111–118. https://www.ncbi.nlm.nih.gov/pubmed/28437710.

[133] G.L. Lokesh, H. Wang, C.H. Lam, V. Thiviyanathan, N. Ward, D.G. Gorenstein, D. E. Volk, X-aptamer selection and validation, Methods Mol. Biol. 1632 (2017) 151–174. https://www.ncbi.nlm.nih.gov/pubmed/28730438.

[134] M.R. Dunn, C.M. McCloskey, P. Buckley, K. Rhea, J.C. Chaput, Generating biologically stable TNA aptamers that function with high affinity and thermal stability, J. Am. Chem. Soc. 142 (2020) 7721–7724, https://doi.org/10.1021/jacs.0c00641.

[135] F. Tolle, M. Rosenthal, F. Pfeiffer, G. Mayer, Click reaction on solid phase enables high fidelity synthesis of nucleobase-modified DNA, Bioconjugate Chem. 27 (2016) 500–503. https://www.ncbi.nlm.nih.gov/pubmed/26850226.

[136] M.S. Singh, S. Chowdhury, S. Koley, Advances of azide-alkyne cycloaddition-click chemistry over the recent decade, Tetrahedron 72 (2016) 5257–5283. http://www.sciencedirect.com/science/article/pii/S0040402016306792.

[137] J.A. Doudna, The promise and challenge of therapeutic genome editing, Nature 578 (2020) 229–236. https://www.ncbi.nlm.nih.gov/pubmed/32051598.

[138] S. Zhen, Y. Takahashi, S. Narita, Y.C. Yang, X. Li, Targeted delivery of CRISPR/Cas9 to prostate cancer by modified gRNA using a flexible aptamer-cationic liposome, Oncotarget 8 (2017) 9375–9387. https://www.ncbi.nlm.nih.gov/pubmed/28030843.

[139] C. Liang, F. Li, L. Wang, Z.-K. Zhang, C. Wang, B. He, J. Li, Z. Chen, A.B. Shaikh, J. Liu, X. Wu, S. Peng, L. Dang, B. Guo, X. He, D.W.T. Au, C. Lu, H. Zhu, B.-T. Zhang, A. Lu, G. Zhang, Tumor cell-targeted delivery of CRISPR/Cas9 by aptamer-functionalized lipopolymer for therapeutic genome editing of VEGFA in osteosarcoma, Biomaterials 147 (2017) 68–85. http://www.sciencedirect.com/science/article/pii/S0142961217305781.

[140] L. Xu, Q. Dai, Z. Shi, X. Liu, L. Gao, Z. Wang, X. Zhu, Z. Li, Accurate MRSA identification through dual-functional aptamer and CRISPR-Cas12a assisted rolling circle amplification, J. Microbiol. Methods 173 (2020) 105917. http://www.sciencedirect.com/science/article/pii/S0167701220300227.

[141] W.-H. Kong, Y. Li, M.-W. Peng, D.-G. Kong, X.-B. Yang, L. Wang, M.-Q. Liu, SARS-CoV-2 detection in patients with influenza-like illness, Nature Microbiol (2020), https://doi.org/10.1038/s41564-020-0713-1.

[142] S.M. Kissler, C. Tedijanto, E. Goldstein, Y.H. Grad, M. Lipsitch, Projecting the transmission dynamics of SARS-CoV-2 through the postpandemic period, Science (2020) eabb5793, http://science.sciencemag.org/content/early/2020/04/14/science.abb5793.abstract.

[143] S.J. Cho, H.M. Woo, K.S. Kim, J.W. Oh, Y.J. Jeong, Novel system for detecting SARS coronavirus nucleocapsid protein using an ssDNA aptamer, J. Biosci. Bioeng. 112 (2011) 535–540. https://www.ncbi.nlm.nih.gov/pubmed/21920814.

[144] D.G. Ahn, I.J. Jeon, J.D. Kim, M.S. Song, S.R. Han, S.W. Lee, H. Jung, J.W. Oh, RNA aptamer-based sensitive detection of SARS coronavirus nucleocapsid protein, Analyst 134 (2009) 1896–1901. https://www.ncbi.nlm.nih.gov/pubmed/19684916.

[145] K.T. Shum, J.A. Tanner, Differential inhibitory activities and stabilisation of DNA aptamers against the SARS coronavirus helicase, Chembiochem 9 (2008) 3037–3045. https://www.ncbi.nlm.nih.gov/pubmed/19031435.

[146] K.J. Jang, N.R. Lee, W.S. Yeo, Y.J. Jeong, D.E. Kim, Isolation of inhibitory RNA aptamers against severe acute respiratory syndrome (SARS) coronavirus NTPase/Helicase, Biochem. Biophys. Res. Commun. 366 (2008) 738–744. https://www.ncbi.nlm.nih.gov/pubmed/18082623.

[147] R. Rangan, A.M. Watkins, W. Kladwang, R. Das, De novo 3D models of SARS-CoV-2 RNA elements and small-molecule-binding RNAs to guide drug discovery, bioRxiv 2020 (2020), 2004.2014.041962. https://www.biorxiv.org/content/biorxiv/early/2020/04/15/2020.04.14.041962.full.pdf.

[148] T.R. Abbott, G. Dhamdhere, Y. Liu, X. Lin, L. Goudy, L. Zeng, A. Chemparathy, S. Chmura, N.S. Heaton, R. Debs, T. Pande, D. Endy, M.F. La Russa, D.B. Lewis, L. S. Qi, Development of CRISPR as an antiviral strategy to combat SARS-CoV-2 and influenza, Cell (2020), https://doi.org/10.1016/j.cell.2020.04.020.